2008

A computational study of quasi-2D flows at low Reynolds numbers

Haiyang Gao
Iowa State University

A computational study of quasi-2D flows at low Reynolds numbers

by

Haiyang Gao

A thesis submitted to the graduate faculty

in partial fulfillment of the requirements for the degree of

MASTER OF SCIENCE

Major: Aerospace Engineering

Program of Study Committee:
Z. J. Wang, Major Professor
Hui Hu
Richard Pletcher

Iowa State University

Ames, Iowa

2008

TABLE OF CONTENTS

LIST OF FIGURES iii

LIST OF NOMENCLATURE v

ABSTRACT vi

CHAPTER 1 INTRODUCTION 1

1.1 Low-Reynolds-number Flow and Its Application 1
1.2 Features of Low-Reynolds-number aerodynamics 2
1.3 Previous Researches on Low Reynolds Number Aerodynamics 5
1.4 About the present study 8

CHAPTER 2 PROBLEM ANALYSIS AND NUMERICAL METHODS 10

2.1 Physics of the Flow under Investigation 10
2.2 Numerical Methods 11

CHAPTER 3 NUMERICAL SIMULATION FOR FLOW AROUND A SMOOTH AIRFOIL 17

3.1 2D Simulation 17
3.2 3D Simulation 30
3.3 Discussion of the 2D Navier-Stokes Solution 34

CHAPTER 4 NUMERICAL SIMULATION OF A CORRUGATED DRAGONFLY AIRFOIL 42

4.1 Airfoil Geometry and Meshes 42
4.2 Numerical Verification Study 43
4.3 2D Simulation Results 46
4.4 3D Simulation of Corrugated Dragonfly Airfoil @AOA=16 deg 47

CONCLUSIONS AND FUTURE WORK 50

BIBLIOGRAPHY 51

LIST OF FIGURES

Figure 1-1	Reynolds number spectrum of flights	2
Figure 1-2	Transitional separation bubble	4
Figure 1-3	NASA low-speed GA(W)-1 Airfoil	8
Figure 1-4	Corrugated Dragonfly Airfoil	9
Figure 2-1	Structured grids for smooth airfoil used in grid refinement study	15
Figure 3-1	Time-averaged Pressure coefficient distribution computed on the three grids	18
Figure 3-2	Grid configurations in the verification of computational domain size	19
Figure 3-3	Lift coefficient history of original grid and the grid with extended boundary	19
Figure 3-4	Time step verification study	20
Figure 3-5	Implicit Inner iteration convergence verification study	20
Figure 3-6	Verification study on types of boundary condition	21
Figure 3-7	Solver verification: lift coefficient history computed by MUSIC and FLUENT	22
Figure 3-8	Averaged Lift Coefficient: CFD vs. Wind Tunnel Tests	22
Figure 3-9	Pressure Coefficient Distribution @AOA=6 deg	23
Figure 3-10	Computed Time-averaged Streamline @AOA=6 deg	24
Figure 3-11	Transient Vorticity Contours @AOA=6 deg	24
Figure 3-12	Pressure Coefficient Distribution @AOA=9 deg	25
Figure 3-13	Computed Time-averaged Streamline @AOA=9 deg	26
Figure 3-14	Transient Flow Field @AOA=9 deg	26
Figure 3-15	Verification of 16deg AOA case with different grids and solvers: Lift coefficient history	27
Figure 3-16	Computed Time-averaged Streamline @AOA=16 deg	28
Figure 3-17	PIV measured flow field @AOA=15deg	28
Figure 3-18	Computed pressure coefficient distribution @AOA=16 deg	29
Figure 3-19	Computed Transient Vorticity Contours	29
Figure 3-20	Lift Coefficient History, 2D CFD vs. 3D CFD	31
Figure 3-21	Computed Time-averaged Streamline @16deg AOA	32

Figure 3-22	Transient Vorticity Iso-surface colored by Mach number	32
Figure 3-23	Lift coefficients, CFD vs. Experiment, CFD computed by 2D and 3D simulation	33
Figure 3-24	Computed Unsteady Vortex Motion @AOA= 0deg	34
Figure 3-25	Comparison of transient vorticity contours by 2D simulation and 3D simulation (median-span plane) @AOA=16 deg	36
Figure 3-26	Time-averaged velocity contours from 2D simulation	38
Figure 3-27	Vorticity iso-surface colored by gauge pressure @AOA=16 deg	38
Figure 3-28	Vorticity iso-surface colored by gauge pressure @AOA=16 deg	39
Figure 3-29	Vorticity iso-surface colored by gauge pressure @AOA=4 deg	40
Figure 3-30	Vorticity iso-surface colored by gauge pressure @AOA=10 deg	40
Figure 4-1	The geometry of the dragonfly airfoil	42
Figure 4-2	Coarse and Fine meshes of dragonfly airfoil	43
Figure 4-3	The lift coefficient history computed by MUSIC with coarse and fine meshes	44
Figure 4-4	The lift coefficient history computed by 3rd order spectral difference solver with coarse and fine meshes	44
Figure 4-5	Geometry modification for testing the numerical uncertainty by ideal sharp corners	45
Figure 4-6	C_L comparison between the sharp corner and blunt corner geometry	45
Figure 4-7	2D CFD time-averaged lift coefficients compared with experimental results	46
Figure 4-8	Instantaneous vorticity field by 2D simulation	47
Figure 4-9	Comparison of lift coefficients history @ AOA=16 deg by 2D and 3D simulation by MUSIC	48
Figure 4-10	Lift coefficients history @ AOA=16 deg from 3D simulation by 3rd order spectral difference	48
Figure 4-11	Instantaneous vorticity field by 3D simulation of 3rd order spectral difference solver	49

LIST OF NOMENCLATURE

C_p	=	pressure coefficient
C_L	=	lift coefficient
Re	=	Reynolds number
Re_c	=	chord-based Reynolds number
c	=	chord length
t	=	physical time
v	=	dynamic viscosity coefficient
u	=	velocity
ω	=	vorticity
x	=	Cartesian coordinates
p	=	pressure
i, j	=	tensor indices

ABSTRACT

Previous studies on low Reynolds number quasi-2D flow around airfoils were mostly two-dimensional, with issues for stalling behavior at higher angles of attack (AOAs). In the present work, a computational study was conducted to investigate the unsteady quasi-2D flow around a streamlined NASA low-speed GA(W)-1 airfoil and a corrugated dragonfly airfoil at the Reynolds numbers of 68,000 and 55,000 with both 2D and 3D simulations. These simulations were carried out by solving the unsteady 2D and 3D Navier-Stokes equations to predict the behavior of the unsteady flow structures around the airfoils at different AOAs. Extensive comparisons were made between the numerical results and wind-tunnel experimental results for the same configurations. It was found that the 2D and 3D simulations differ significantly at relatively high AOAs, and that the 3D computational results agree much better with the experimental data. It is believed that unsteady vortex-dominated flow at high angle of attack is strongly three-dimensional. As a result, the 2D simulations are not adequate in resolving the fundamental flow physics, and 3D simulations are necessary to correctly predict the flow behavior at such conditions.

Chapter 1

Introduction

1.1 Low-Reynolds-number Flow and Its Application

Recently, there has been intensive research effort on the low-Reynolds-number flow over man-made and natural flyers, based on the wide application of these types of flows in both military and civil areas.

The need of more knowledge of low-Reynolds-number flow was probably introduced by the study of UAVs (Unmanned Aerial Vehicles), operating in the regime where chord based Reynolds number ranged between 200,000~500,000, and it was also realized that the miniature of conventional airfoils, designed mainly for flow with chord Re larger than 10^7, are likely to have poor performances in this regime [1].

Then in the late 1980s, the idea that a new kind of "tiny aircraft" might also have important uses arose. MAVs (Micro air vehicles), developed out of "miniature UAVs", are referred to as flight machines with dimension of approximately 15 cm and operates at a speed of the order of 10 m/s, and are expected to serve roles such as reconnaissance, communicating, search and rescue, etc. Due to the smaller size of MAVs, they usually operate at an even lower Reynolds number than UAVs. There have been many explorations of various smart designs of MAVs using fixed wings [2, 3], flapping wings [4, 5] and rotary wings, and for each kind of wings, either rigid materials or flexible materials can be used. From another interpretation of Re_c [6],

$$\mathrm{Re}_c = \frac{2c}{\mu V}\frac{1}{C_L}\frac{L}{S}$$

It can be easily seen that MAVs, normally with high lift coefficient and low wing load, easily falls into the low-Reynolds-number realm.

In addition, the low-Reynolds-number regime is also the flow regime for most biological flight, including birds with $\mathrm{Re}=10^4$—10^5, and various insects with $\mathrm{Re}< 10^4$ [7], and the flight of these living creatures has always been a fascinating topics for fluid mechanics research, which also requires more profound understanding gained on low-Reynolds-number flow (see Figure 1-1).

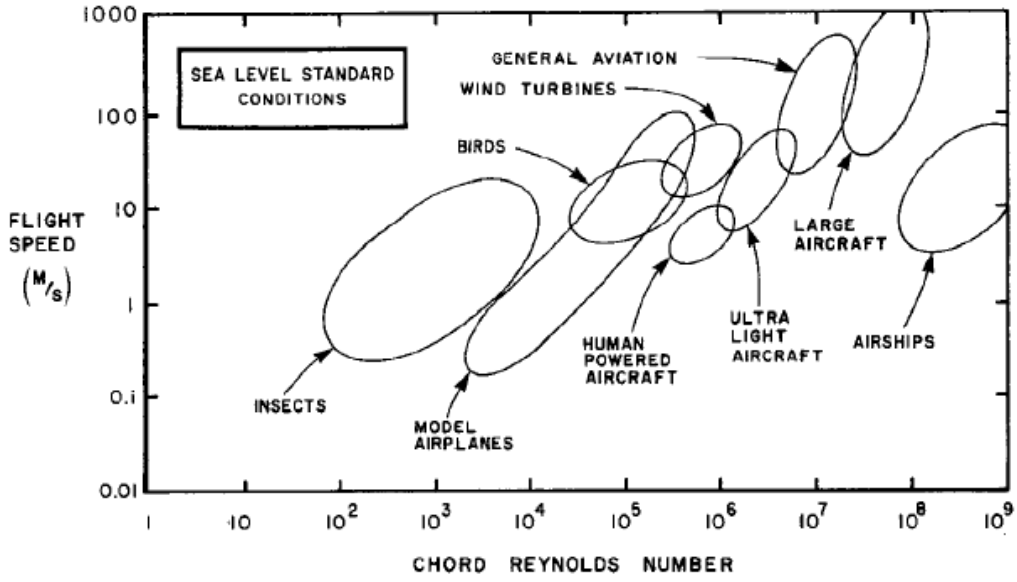

Figure 1-1: Reynolds number spectrum of flights [7]

1.2 Features of Low-Reynolds-number Aerodynamics

Generally, there are 3 Reynolds number regimes. The first regime is one which is dominated by viscous forces, as small organisms wiggle through the fluid, and the third is one that is dominated by inertial forces, with inviscid characteristic wakes in the outer flow. The second regime, is where the so-called "low Reynolds number flow" falls into, and is one that is difficult to study with all kinds of complex flow attributes [8].

As we can see, the term "low-Reynolds-number flow" usually does not refer to the flow with very low Reynolds numbers, but rather refers to the flow with relatively lower Reynolds numbers than conventional aircraft aerodynamics, i.e. $\mathrm{Re}_c > 10^7$. Although this regime is normally taken to be $\mathrm{Re}_c = 10^3 \sim 5\times10^5$, in a specific aerodynamic study, it is really dependent on the object in question. Normally, in studies on UAVs, people will assume $\mathrm{Re}_c = 2\times10^5 \sim 5\times10^5$ [9], similarly $\mathrm{Re}_c = 10^4 \sim 10^5$ for the studies related to MAVs, and when it comes to the studies of insect flights, it easily falls into the regime $\mathrm{Re}_c < 10^4$ [10].

Since there is no clear and fixed range of Reynolds number to define a low-Reynolds-number flow, but only some guidelines numbers, the question comes up what defines a flow to be in low-Reynolds-number regime. The answer to this question lies in the flow features.

Normally in a lift generating surface, there must a region where the pressure is lower than the static pressure of the incoming fluid, and the region with the lowest pressure is the so-called "suction peak" in the upper surface of the airfoil or wing. After the suction peak, the pressure will go up and will finally be close to the static pressure of the incoming flow near the trailing edge, and this process is called "pressure recovery", in which the flow deals with an adverse pressure gradient. In a conventional high Reynolds number flow, the flow will quickly make the transition from laminar flow to turbulence well before it comes across strong adverse pressure and the strong energy transfer of turbulence helps negotiating the pressure gradient and thus makes the pressure recovery more of an attached manner. However, when the Reynolds number is lower, it may stay laminar when the flow goes into the adverse pressure gradient and is subjected to a laminar separation [8]. Usually the flow separates before transition is referred to as a low-Reynolds-number flow and thus laminar separation is the key feature of the low-Reynolds-number regime.

Except for the cases with lowest Reynolds number in this regime, the flow will undergo the transition to turbulence right after the laminar separation, and with the energy provided by the turbulence energy transfer, the flow will reattach to the wall. This forms the transitional separation bubble (Figure 1-2), which is the most studied structure in low Reynolds number regimes. It is a complex flow structure because it incorporates separation, transition and reattachment within a short distance along the lift surface, and it is also has substantial influence to the lift coefficient of the airfoil or wing under investigation. Besides, transitional separation bubbles are highly sensitive to a large variety of flow parameters, especially the Reynolds number, which makes the flow in low Reynolds number regime highly Re-dependent [11,12]. Therefore, certain range of Reynolds number in this regime may have its unique flow feature, and thus when dealing with low-Reynolds-number aerodynamics, researchers should pay attention to the Reynolds number in question, and caution must be taken in comparison of different sets of data too. And this is the reason of the disparity of the range of Reynolds number of various studies mentioned above.

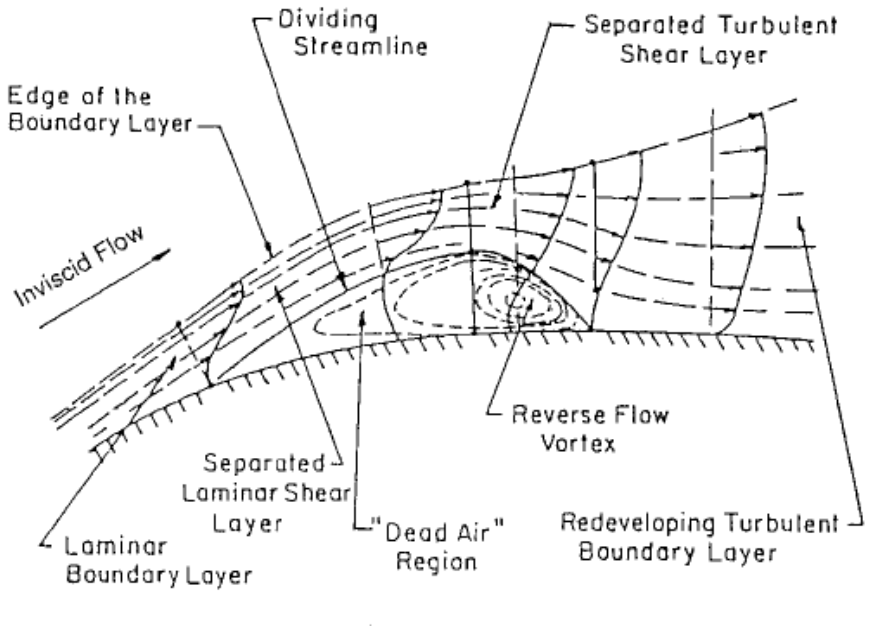

Figure 1-2: Transitional separation bubble [38]

Although it does not happen in all Reynolds numbers or all angles of attack (AOAs), the transitional separation bubble dictates the aerodynamics performance of low Reynolds number airfoils and wings. And since it is so much emphasized in various studies, it is almost the "signature" of low Reynolds number regime. However, we should be aware of the fact that transitional separation bubble does occur in some high Reynolds number flows too, but in that case their length is only about 2% of the chord length and thus they have almost no effect on the overall aerodynamics performance [13] (transitional separation bubbles can be as long as 15% of chord length in low Reynolds number flows).

After the flow goes through the laminar separation bubble and becomes turbulent, it is also possible for the flow to encounter a secondary turbulent separation bubble [14], but the smaller size and longer distance from the suction peak make this kind of separation bubble less important in the study of aerodynamic performances.

Huang and Lin (1996) [37] gave a clear chart of the complication of low Reynolds number flow. Basically, flow is unsteady, involves significant separation phenomenon, and 3D effects frequently come into play. And with different Reynolds number ranges, completely different flow field can be developed. And for the Reynolds number of the current study, the chart showed that it should be an unsteady flow in lower AOAs and a 3D unsteady flow in higher AOAs.

1.3 Previous Researches on Low Reynolds Number Aerodynamics

Numerous research projects have been conducted related to the low Reynolds number regime, which mainly falls into three categories: experimental studies, numerical studies and the design philosophy of airfoils and wings.

Early wind tunnel experiments, due to the limit of conventional measurements are often conducted under the assumption that the flow is steady, and only time-averaged flow features are measured with some crude visualization techniques to reveal parts of the unsteady nature. These approaches, although omitting some unsteady natures, actually do make some sense because the aerodynamic performance of an airfoil largely depends on the time-averaged features [15]. And this leads to the fact that knowledge on the flow structures and concepts such as separation bubbles and burst of bubbles are all in the time-average sense.

And it is discovered that there were a lot of inconsistencies in the data acquired in different experimental studies, e.g. Nagamatsu and Cuche (1980)[16] revealed that lift coefficients were insensitive to the change of Reynolds number, while several other studies clearly suggested substantial dependence of lift and drag on Reynolds numbers[11, 17]. And Marchman (1987)[14] did a general study on the accuracy of wind tunnel tests on the low Reynolds number regime and found that this regime of flow were sensitive to all kinds of experimental parameters, especially turbulence intensity of incoming flow and acoustic disturbance. Pelletier and Mueller (2001)[18] even suggested the different configuration of the end plates in quasi-two-dimensional tests might also have some significance to the outcome of the experimental results, and he also suggested probable high influence of 3D structures.

The transitional separation bubble is certainly under the spotlight of the experimentalists, with its importance well recognized. Brendel and Mueller (1988)[13] did an exclusive research on the boundary layer parameters in the vicinity of the transitional separation bubble, and in most other experimental studies, the separation bubble was carefully observed and its behavior was heavily related to the overall performance of the airfoil.

Broeren and Bragg (2001) [19] was one of the studies that investigates the three dimensional effects in a quasi-two-dimensional airfoil flow, which showed that 3D structure “stall cells” only existed in trailing edge separation, which was likely to cause a gradual stall. But for those airfoils with leading edge separation, which will cause in sudden loss of lift when stalling, the structure is mainly 2D. This view was also claimed in the study of Marchman III and Abtahi (1985) [6], stating that the flow structure in the tested airfoil is mostly 2D. However, all the claims above were based on the measurement

of the mean velocity along the spanwise direction. When mean velocity shows little variation along the span, it is quite possible that the transient flow field is much involved with 3D effects, so this conclusion needs further investigation.

Other experimental research included low Reynolds number wings under different practical conditions, such as in fluctuating incoming flow [20], in rainy weather [21], full MAV wind tunnel test with the application of vertical stabilizer in the tail section [22], multi-wing system in low Reynolds number [23], and airfoil performance with flapping-like motions [10]. These studies provided useful lift and drag data, but did not uncover much of the underlying physics.

Recently, with newer experimental techniques available, more detailed measurements have been made. Hu and Yang (2007) [15] did extensive tests on GA(W)-1 airfoil and revealed the unsteadiness of the real flow field, and an analysis of the physics underlying the low Reynolds number phenomenon, and it also makes a good benchmark test for numerical simulations.

Numerical studies on low Reynolds number flow have also gone a long way, especially for various 2D low-speed airfoils. The challenge for low Reynolds number flow is that the normally valid assumption of a steady, attached and fully turbulent flow no longer holds. Transition region is much larger in this regime, and it also involves much more complicated flow patterns, the traditional way of using corrections to deal with transition [24] is unlikely to work, and due to its crucial influence on the whole flow field and the overall performance of the airfoil or wing, the transitional separation bubble must be taken into account of in the simulation. Besides, it has been shown that standard turbulence models often fail to work as well as in conventional high-Reynolds number regimes. Therefore, the low-Reynolds number turbulence modeling is less mature with many undecided issues to solve [34], and models and the coefficients involved in the modeling are more problem-dependent.

Earlier research, limited by the computing power, normally did not utilize full Navier-Stokes simulations, but used some inviscid-viscous interaction techniques. In term of the simulation of transitional bubble, semi-empirical models are widely used to predict the location and the flow near the transition point [25, 26]. The drawback of these methods is obvious. First, as is mentioned above, the low Reynolds number flow is highly dependent on the Reynolds number, and using these models often involves choosing a lot of empirical constants. Therefore, the volatile nature of the flow will make it hard for any set of constants to have much generality, thus the constants will be rather problem-dependent [11]. Another problem with these methods is that they deal with the transitional

separation bubble locally, which neglects its global effects on the whole flow field, and it certainly cannot predict large scale separations and post stall behavior of the flow [26].

More advanced methods were used later. One idea is to use linear stability theory, i.e. e^N method, to predict the location of the transition, and use an eddy-viscosity based turbulence model in the region after transition. This method has been used in both airfoils [27] and 3D wings with a sweep angle [28]. Another idea combines the linear stability theory in transition location prediction and a family of "separation bubble model" designed specifically for transitional separation bubbles, which is able to obtain a good agreement in bubble sizes and velocity gradients [29, 12]. More recently, with the increase of computing power, Lian and Shyy (2007) [30] have used the N-S simulation plus a transition model for low Reynolds number flows in a 2D simulation, acquiring good agreements up to the stall AOAs on an airfoil characterized by a trailing edge stall type. However, none of the studies above succeeded in predicting the right post-stall trend.

The studies above were all attempting to get the solution of low Reynolds number flows in a steady manner, and what they are finally getting is again, time-averaged flow fields. Lin and Pauley (1996) [38] conducted an unsteady simulation of an 2D airfoil in a low Reynolds number, which revealed that underlying the attached time-averaged flow, there was a successive vortex shedding behavior near the trailing edge, which agreed with Hu et al 's PIV visualization [15]. Besides, an early full incompressible Navier-Stokes simulation was conducted in 2D with vorticity-streamfunction formulation of N-S equation, aiming to resolve as much flow details as possible without the use of any turbulence models, and unsteady vortical structures were also discovered [31]. However, the post-stall trend is still not correctly predicted in neither study.

In the meantime, various design philosophies for low Reynolds number airfoils have been developed. Various specially designed low Reynolds number airfoils [32, 33, 35] turned out to be able to offer much better performance than conventional airfoils. These designs have more or less something to do with the transitional bubble structure in the upper surface, e.g. the use of a "transition ramp" to promote the transition without introducing large bubbles [9], and the introduction of concave pressure recovery and aft loading to redistribute the load [36]. However, the incomplete understanding of transition process greatly impedes the development of newer airfoils.

1.4 About the present study

As can be seen, most studies on quasi-two-dimensional airfoil flow are performed with 2D simulations, with the seemingly reasonable assumption that a 2D CFD simulation is

enough to describe the flow field. But the low Reynolds number flow itself is possibly full of large scale 3D unsteady votical structures, and the question remains open whether a 2D simulation is sufficient to get a close enough solution and describe the flow field correctly, with precise prediction of aerodynamic performances like lift and drag coefficients.

In the present study, a numerical validity test was performed to test the proficiency of a 2D Navier-Stokes simulation, with a systematic way to eliminate the numerical uncertainties from various sources. Then, a 3D simulation was performed to further verify the conclusion and analyze the role played by 3D structures. Both 2D and 3D CFD results were compared with the experimental measurements of the same configurations and Reynolds numbers.

The studies were performed on two kinds of airfoils: the first is a NASA low-speed GA(W)-1 airfoil (Figure 1-3) with the Reynolds number of 68,000, which is a conventional smooth airfoil which is specially designed for low Reynolds number applications; the other is a corrugated dragonfly airfoil (Figure 1-4) whose profile is from a dragonfly wing, with the Reynolds number of 55,000.

The author hopes to find ways to predict the low Reynolds number flow behavior more accurately with reasonable amount of computing. Besides, this study explores the higher AOA post-stall region, which has caused the most discrepancies in previous numerical studies. And by revealing the essential unsteady nature underlying the previously recognized time-averaged behaviors, further investigations were made towards the understanding of low Reynolds number phenomenon.

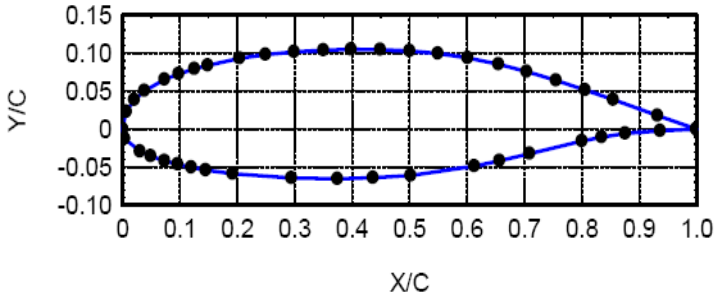

Figure 1-3 NASA low-speed GA(W)-1 Airfoil

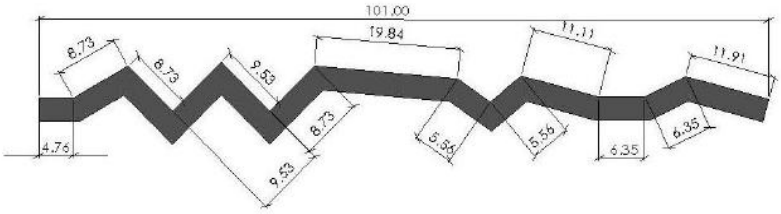

Figure 1-4 Corrugated Dragonfly Airfoil

Chapter 2

Problem Analysis and Numerical Methods

2.1 Physics of the Flow under Investigation

The smooth airfoil under investigation is the GA (W)-1 airfoil, also known as NASA LS(1)-0417 (Figure 1-3), which is specifically designed for low speed aviation applications with a large leading-edge radius to mitigate the pressure peak to discourage separation. The maximum thickness of the airfoil is 17%.

The reference data for this study is from the experiment by Hu et al (2007) [15], which was conducted in a closed-circuit low-speed wind tunnel in Iowa State University, with special devices for reducing turbulence intensity. A typical 2D test model was used, with two endplates at the wall of the wind tunnel and pressure measurements taken in the median span of the test model, and the data from 43 pressure taps was integrated for lift and drag coefficients. The Reynolds number of the

The pressure measurement here is not of too much difference compared with other experiments on airfoils, the mean pressure coefficients are obtained and thus the time-averaged lift and drag coefficients are measured. Due to the uncertainty of measurement, the relative error of lift coefficients here is much smaller, so all the comparisons are made in lift coefficient rather than the drag coefficient.

PIV measurements were also conducted to reveal the transient as well as mean detailed flow feature, also in the mid-span plane, and it is a very reasonable assumption that the time average of this flow field represents that of an ideal 2D airfoil.

The time-averaged performance of the airfoil can be divided into 3 regions: the attached flow region (AOA<7 deg), separation bubble region (AOA=7~11 deg), and the post-stall region (AOA>11 deg). A linearly increasing lift coefficient was obtained in the attached flow region. At AOA≈8, the transitional separation bubble started to appear, but the suction peak in the nose of the airfoil retained and the pressure peak near the nose of the upper surface kept increasing, besides, the transitional separation bubble formed a plateau in the pressure coefficient, which is also a typical phenomenon. The separation bubble burst at about AOA=11 deg and thus caused an abrupt drop of lift coefficient, in the pressure coefficient, it is represented by the collapse of the suction peak. And very large separation area was found in the mean flow field right after the airfoil stalled.

The stall behavior of this airfoil can be characterized as a leading edge stall, in which the separation bubble forms near the leading edge and grows as the AOA increases, and then

will be subject to a sudden burst at some AOA and thus cause the abrupt downgrade of performance.

The transient behavior of the flow, uncovered by the PIV measurements, shows the universality of unsteadiness under this Reynolds number, as described in [38], successive vortex shedding is present even in the low AOA attached flows, and the flow is dominant by large scale structures.

In the experiment, the lift coefficients when both increasing and decreasing angle of attack were obtained and found to be exactly the same for the same AOA. This means the hysteresis effect, which is common for leading edge stall type, is not present in this test case due to the low Reynolds number. Numerically, this suggests that the solution of this problem should not depend on the initial conditions, which makes it a good benchmark case for testing numerical capability to solve the low Reynolds number problem.

2.2 Numerical Methods

2.2.1 Governing Equations

Although the flow has a relatively chord lower Reynolds number, it is clear that transition to turbulence does play a vital role in the flow field. The computing power available to the author is much less than adequate for a complete simulation such as Direct Numerical Simulation (DNS) or Large Eddy Simulation (LES). Besides, a conventional turbulence modeling is unlikely to work, since in low Reynolds number regime, we cannot assume whole flow field to be turbulence given the conspicuous contribution of the transitional separation bubble. In addition, the standard turbulence models tend to work not as well in this Reynolds number regime.

There are quite a few low-Reynolds-number models available [34, 39], as well as transition models designed to predict the transition point and model the process. But utilizing these models will involve large number of parameters, making it difficult to study the effect of any single factor, let alone the capability of the numerical method. Besides, these models tend to solve the flow to a steady solution or time-averaged solution, while their effectiveness for unsteady flow is not clear.

Therefore, the present study uses pure Navier-Stokes simulation, without using any turbulence models, in the hope of resolve as much structures as possible with reasonable computing power. And thus this study can be viewed as an LES study with the numerical dissipation of the scheme as the sub-grid scale model, though strictly speaking, there is no LES for 2D simulations. The error caused by the current method would from the energy dissipation of the scales smaller than the grid size, which virtually almost remove eddies

of these scales from the flow field. The effect of this will be revisited in later chapters of this study. Besides, the dissipation of the small scale motions might also cause an abnormal increase of energy of the scale close to grid size, which certainly will also cause some errors to the simulation.

Lin and Pauley (1996) [38] suggested that in low Reynolds number flows, the physics are dominated by the large scale vortex structures and smaller scale turbulence only plays a secondary role. They also commented that in the separation region laminar flow is dominant. Whether these claims are valid will be tested in the present study.

2.2.2 Elimination of Numerical Uncertainties

Nowadays, the flow simulation of CFD is still regarded unreliable way without comparing to wind tunnel tests. This predicament is due to the difficulty of error control. In CFD, the worse thing than the existence of error is that it is often difficult, if possible, to estimate the magnitude of error without comparing it to reference experimental results.

The reason for this is that in the whole process of CFD, there are too many sources of numerical uncertainties. There are errors caused by the incapability of solution schemes, by the lack of resolution of the computational grid, by the incorrectly chosen boundary conditions and initial conditions, by a not large enough computational domain, by the error propagation through time marching and so on. Even the equation to be solved may not be adequate for the problem in question, for example the lack of generality of most turbulent models often cause the model being used is not capable of getting the right results in a particular case.

Therefore, it is clearly very important to know whether or not the equation, or the mathematical model of the physics phenomenon, is adequate for problem to be solved. If the equation to be solved is insufficient for the problem, there is no possibility the numerical solution would be accurate, unless other errors are caused to cancel the error caused by the equation, and obviously, this is not the correct way of problem solving.

To verify the capability of a mathematical model in CFD, the most essential thing is to acquire a true numerical solution by eliminating or at least minimizing the numerical uncertainties. Such a numerical solution is one that can represent the maximal capability of the numerical model, and is independent of the mesh, the computational domain size, the time step or CFL number, other parameters of the simulation, and even the solvers. In other words, it is related to only partial differential equations problem, but not on what method is used to solve the problem.

For the current problem, it is intuitive to solve it within a 2D framework, since it is only a 2D airfoil, the flow field of which is supposed to be uniform in the spanwise direction at least in the time-average sense. But based on the fact many previous researches following this direction had troubles especially in post-stall AOAs. The question remains open that whether 2D Navier-Stokes equation is an adequate mathematical model for the flow around a 2D airfoil. And this is the question the present study is trying to answer.

To obtain the answer, it follows that the true numerical solution of the 2D Navier-Stokes equation for this problem must be found, and after ruling out all possible known numerical uncertainties, the discrepancy that is left, if any, is due to incapability of the 2D Navier-Stokes equation itself.

To get the true numerical solution of 2D N-S equation, verification studies must be done for all the known possible and controllable factors in the simulation.

The resolution of the computational grid is a most common factor that may generate numerical uncertainty, and thus grid refinement study is necessary as a typical procedure. Only when little difference is observed between a coarser grid and a finer grid after some reasonable refinement, can the solution be claimed as qualified in grid resolution.

The boundary condition is another important factor to consider, which includes two aspects, the position of the boundary conditions and the type of them. The position refers to the question whether or not the computational domain is large enough so that the constraints at the boundaries would not cause any unphysical behavior in the area of interest, while the type of boundary condition refers to the question what constraints to apply at the boundaries. To deal with former problem, computational grids with various domain sizes were generated to compare against each other for difference. And for the latter problem, different types of boundary conditions are tested for differences. When only negligible change can be observed between cases, the error from boundary conditions can be ruled out.

Time steps, or CFL numbers, are also a possible factor to generate numerical uncertainties when the time step is not small enough to resolve all the motions in the flow field, especially for an unsteady time-accurate simulation. For this, time step refinement study is conducted, in which time step is continuously reduced until the solution doesn’t change.

In addition to the magnitude of the time steps, time integration schemes may cause errors too. In this study, second order implicit scheme is applied, and one parameter of the

scheme is the convergence criteria of inner iterations within one time step. Therefore, various residual tolerances are applied to test the convergence of the scheme.

And above all, the solver itself may introduce errors due to the numerical method used and possible bugs. To rule this kind of error out, the same simulation is performed on different solvers with largely different numerical methods, if the results can coincide with each other, the odds that both solvers get the wrong answer would tiny.

And after the above verification studies, a solution that is very close to the true numerical solution can be obtained, with which the effectiveness of 2D N-S equation can be analyzed.

2.2.3 Simulation Details

Flow Solver

The computation in this paper is mainly performed with MUSIC, a 2^{nd} order finite volume code capable of handling arbitrary meshes [40] for compressible fluid flow. Roe flux difference splitting scheme is used in the convective flux discretization. Two other solvers are utilized in the numerical verification studies, which are Fluent with a SIMPLE pressure-based discretization and a third-order spectral difference solver [41].

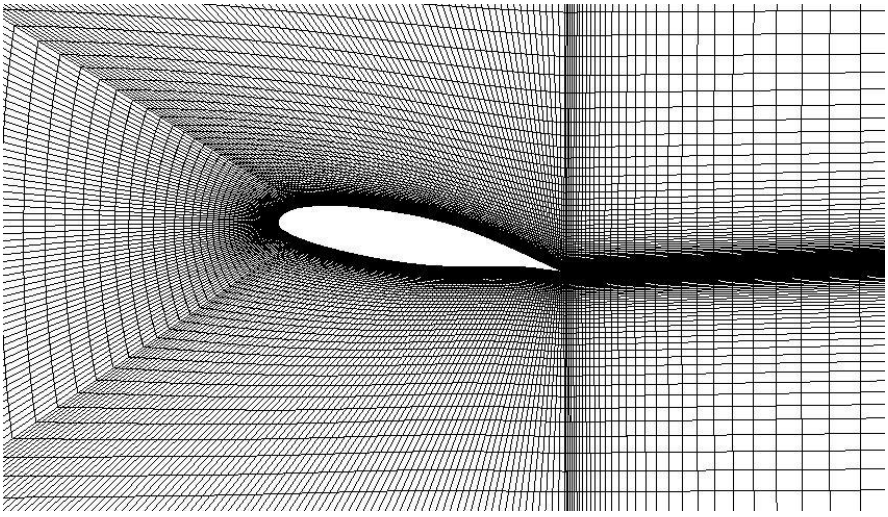

(a)

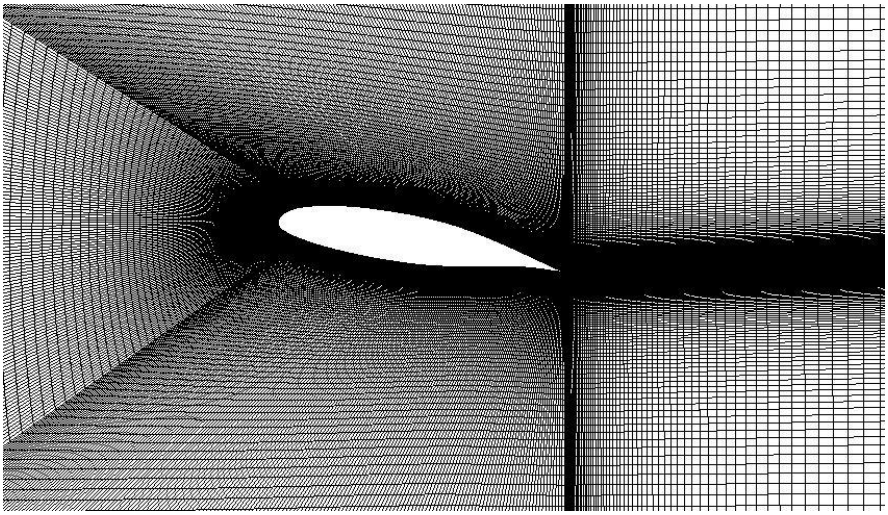

(b)

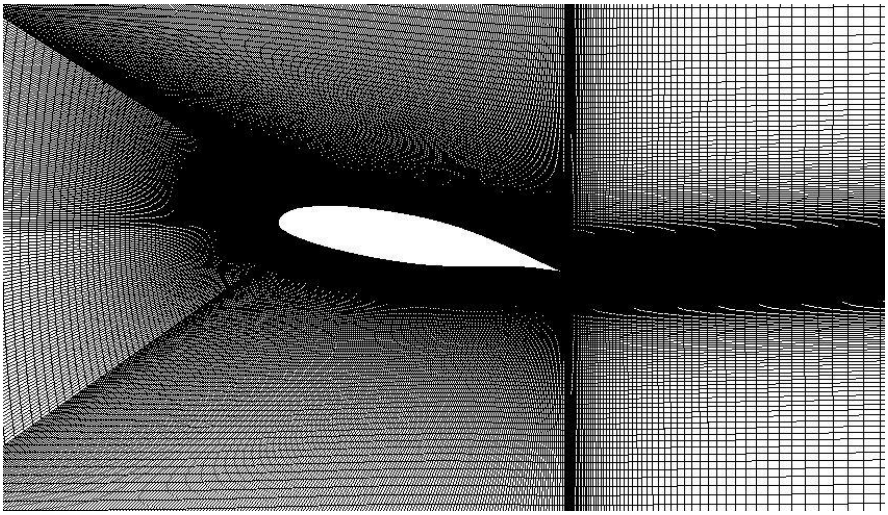

(c)

Figure 2-1: Structured grids for smooth airfoil used in grid refinement study: (a) Coarse (b) Fine (c) Finest

Computational Meshes

Though the MUSIC solver is able to handle arbitrary grid, for the best resolution of the viscous shear flow, C-topology structured grids are used in this study. For grid refinement study, three sets of 2D grid are generated. The coarse mesh has 320×80 cells (Figure 2-2a), the fine mesh with 640×160 cells (Figure 2-2b) and the finest mesh with 860×240 cells (Figure 2-2c).

Initial and Boundary Conditions

As was revealed in the related experiment, there was no hysteresis effect for this airfoil under such low Reynolds numbers, and thus it is reasonable to assume the numerical

solution of the Navier-Stokes equations does not depend on the initial conditions. And thus in this study the initial condition was simply set to the free stream in the whole flow field for all the solvers.

Boundary conditions are sometimes difficult to define if given limited information about the wind tunnel tests. In this study, the boundary conditions used to obtain the final result were: for 2D simulation, everything is fixed at the inlet and pressure was fixed at outlet, with the top and bottom boundaries of the computational domain is applied with symmetric boundary; for 3D simulation, front and back boundaries are also symmetric. Other types of boundary conditions were also used to study what effect the boundary conditions might have on the numerical solution and thus confirm the effectiveness of the selected boundary conditions.

Unsteadiness, Time Integration and Data Averaging

The flow in this case is always unsteady, and all the simulations here need to run with an unsteady time accurate marching scheme. For this purpose, a second order implicit time integration scheme is employed, for each step of the implicit solver, various convergence criteria are also tested for verification.

After the flow reached a periodic state, time-averaged data were obtained for the flow field, pressure coefficient and the lift and drag coefficient to compare with experimental data.

Treatment for the Stiffness Caused by Low Mach number

The wind tunnel tests were run at the speed of about 10 m/s, which corresponds to a Mach number of about 0.03. Because MUSIC is a compressible solver, if the simulations are run at the same Mach number of the experiment, the stiffness caused by the low Mach number is likely to make the computation hard to converge.

And in the numerical simulations, the Mach number was set to 0.2, while corresponding adjustment was made to the viscosity so that the Reynolds number was exactly the same as that of the experiment. Theoretically in an inviscid flow with small perturbation, the error caused by the adjustment above is $1-\sqrt{1-Ma^2} \approx 2\%$, which is not expected to be larger in a viscous flow. This error here is neglected in the study that follows.

Chapter 3

Numerical Simulation for Flow around an Smooth Airfoil

3.1 2D Simulations

Flow simulation in 2D was done in three steps: first, a base case was studied, in which we tested all the numerical parameters and methods, and then comparison are made between a base case and all the control cases, by this, all known types of numerical uncertainties are minimized. Then a verified method, mesh and a set of parameters were chosen. In the second step, the flow under various angles of attack was simulated and comparisons with the experimental results are made. If there were any obvious disagreement, further verification studies were performed in the third step.

The standard for evaluating the effectiveness of a simulation is the statistics, especially the average of lift coefficient and pressure distribution, since it is a practical standard and easy to compare. Besides, the flow field of CFD simulation and PIV measurements were also compared qualitatively.

3.1.1 Verification Studies of the Base Case

The AOA=10 deg case was chosen in this study as the base case, because the lift coefficient is relatively large so that the relative error in the experiment is small, allowing for more precise comparison. Besides, this AOA lies in the range where the flow is dominant by transitional separation bubble, which plays a central role in a low Reynolds number flow, and if this flow is correctly simulated, the method should work well for the most cases.

3.1.1.1 Grid Refinement Study

Simulations were run on the three grids mentioned in the last chapter, for both lift coefficient history and time averaged pressure distribution (Figure 3-1). Time step were chosen just to make the solution converge (CFL number=400), and a fix-everything type inlet boundary condition was used, and the inner convergence stopping criteria was to make the residual drop 2 orders for each time step. As can be seen from Figure 3-1, the fine grid (640×160 cells) came out to a decent grid for computing lift coefficients, and this grid was used in the following verification studies.

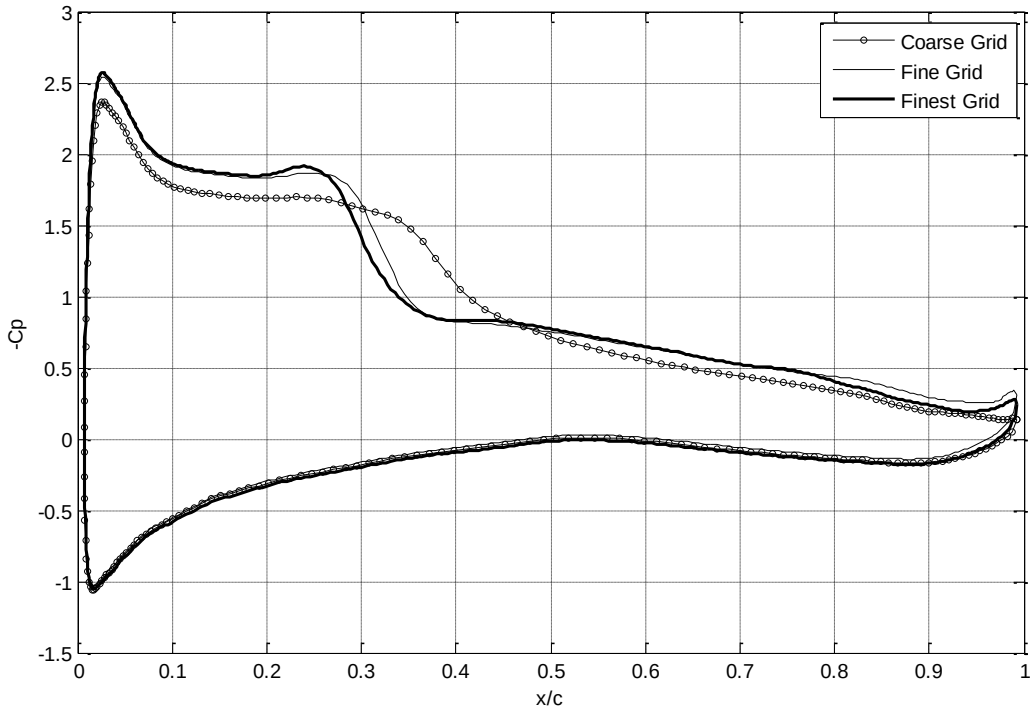

Figure 3-1: Time-averaged Pressure coefficient distribution computed on the three grids

3.1.1.2 Verification of the Size of the Computational Domain

Another grid was generated based on the fine grid, by extending the inlet 2 times chord length upstream and the outlet 2 times chord length downstream (Figure 3-2b). No change was made to the top and bottom boundary because it already was about the same size of the wind tunnel. The simulation result was compared to that for the fine grid in 3.1.1. Figure 3-3 showed that the original computational domain is large enough since little change was observed in time-averaged lift coefficients.

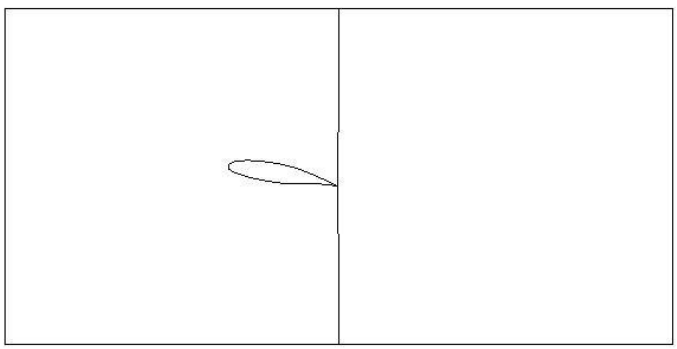

Figure 3-2 (a.) Original grid

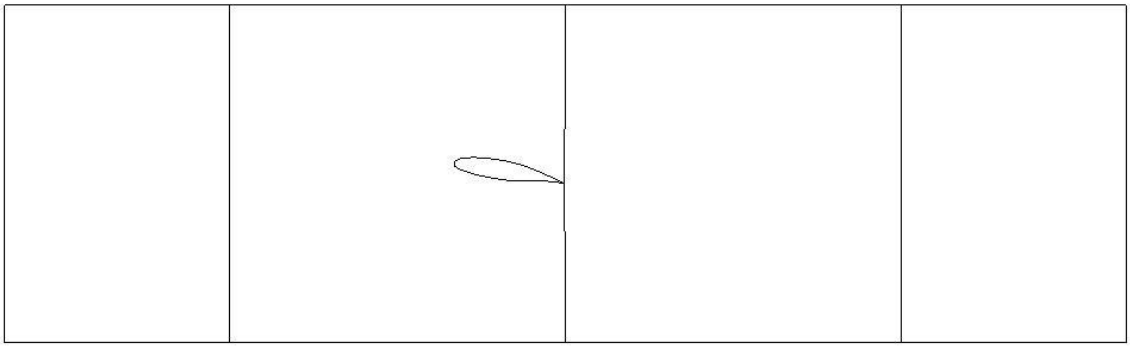

Figure 3-2 (b.) Grid with extended boundary for inlet and outlet

Figure 3-2: Grid configurations in the verification of computational domain size

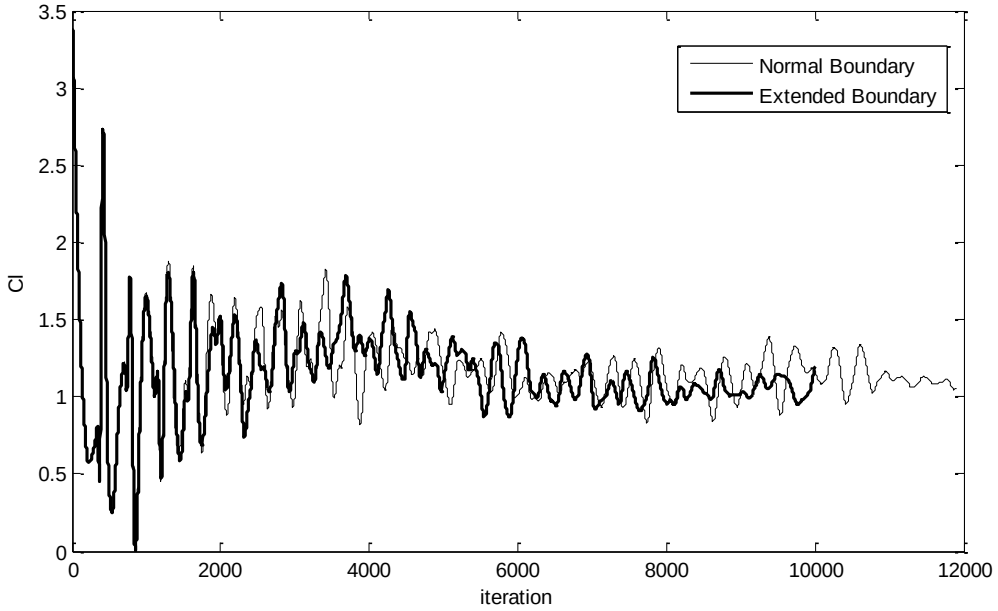

Figure 3-3: Lift coefficient history of original grid and the grid with extended boundary

3.1.1.3 Time step/CFL Verification

The fine grid result from 3.1.1 was compared with that from a simulation using half the time step, and Figure 3-4 showed that the time step was good enough to compute the average aerodynamic performance.

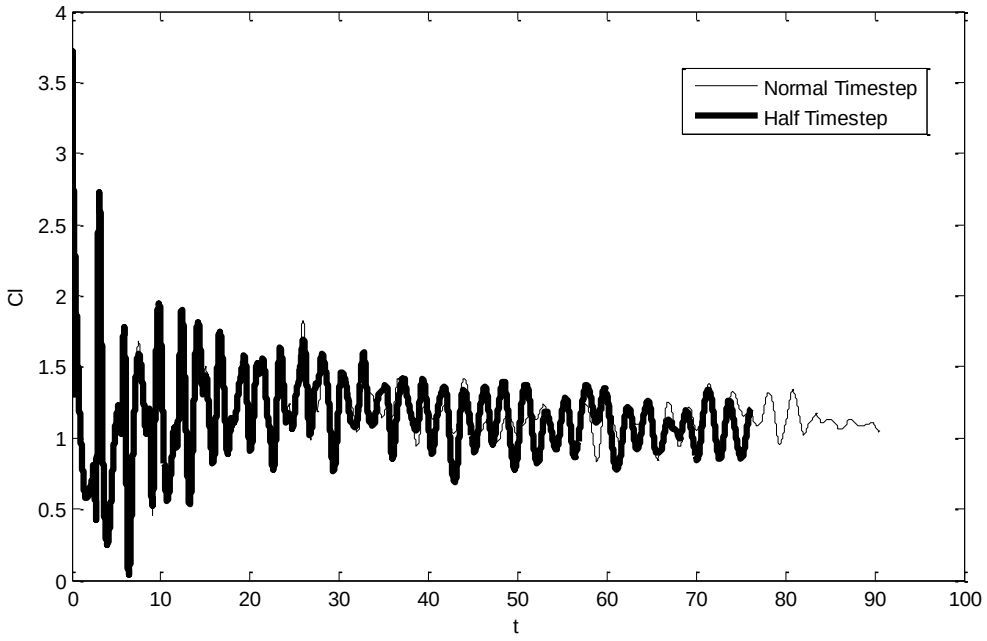

Figure 3-4 Time step verification study:
Lift coefficient history of same grid with 2 time steps

3.1.1.4 Verification of Inner Iteration Convergence for the Implicit Scheme

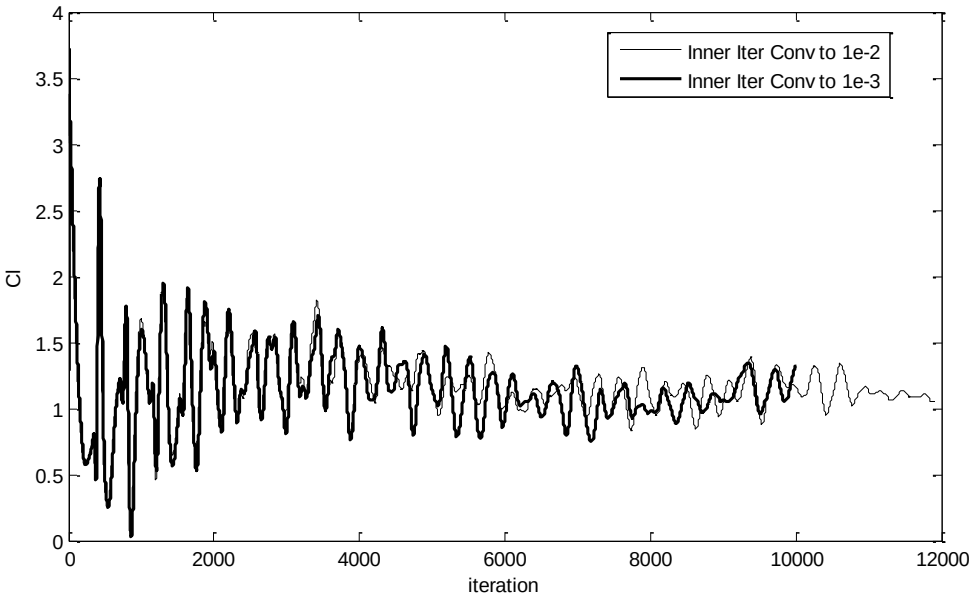

Figure 3-5 Implicit Inner iteration convergence verification study:
Lift coefficient history of two convergence criteria

The fine grid result from 3.1.1 was compared with that from a simulation with inner iteration dropping 3 orders of residual, and Figure 3-5 showed that little change was observed after a stable state had been achieved.

3.1.1.5 Verification of Types of Boundary Condition

A characteristic farfield boundary constraint was applied at the inlet, and the result was compared against the fine grid results from 3.1.1, no big change in the average behavior of the lift coefficient, suggesting that the types of boundary condition would not cause dramatic error and the fix-all inlet was to be used in later simulations (Figure 3-6).

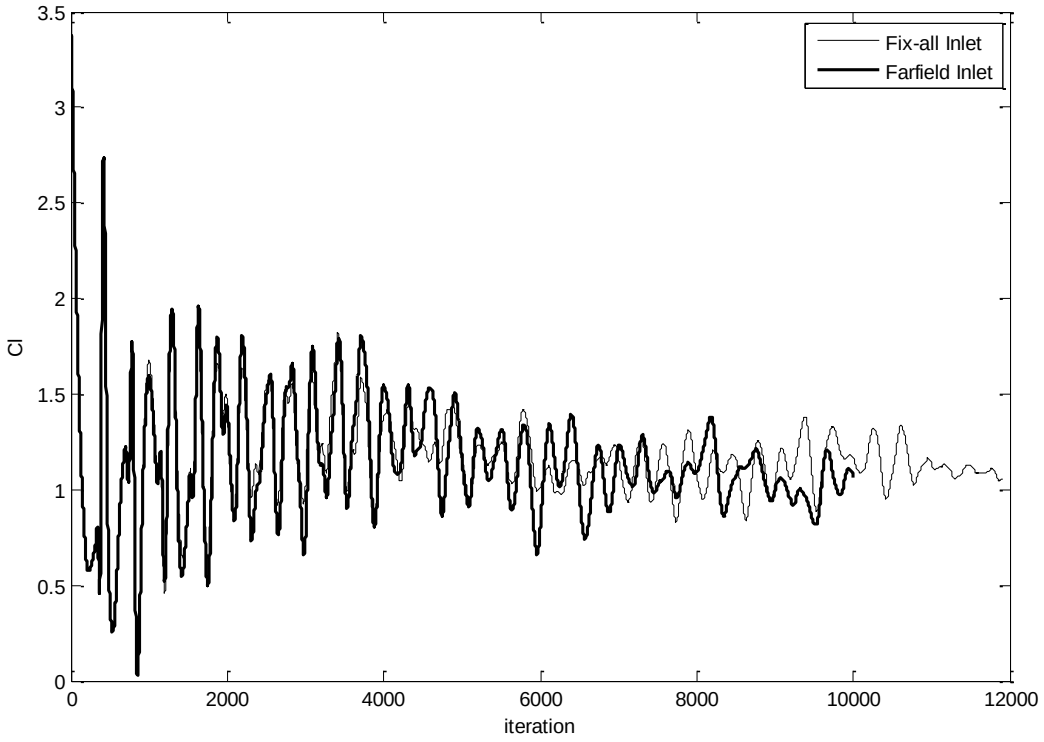

Figure 3-6: Verification study on types of boundary condition: as long as reynolds number was kept unchanged, different types of boundary conditions did not make a big difference in average lift coefficient.

3.1.1.6 Solver Verification

The above results were all from MUSIC, and in Figure 3-7, the result from 3.1.1 was compared with that from a pressure-based incompressible solver from FLUENT. The results, although showed quite some difference initially, finally converged to two very similar solutions, and the average lift is about the same. This results was a very sound proof that the results from both solvers were correct, since the chance that two completely solvers converged to the same wrong solution was tiny.

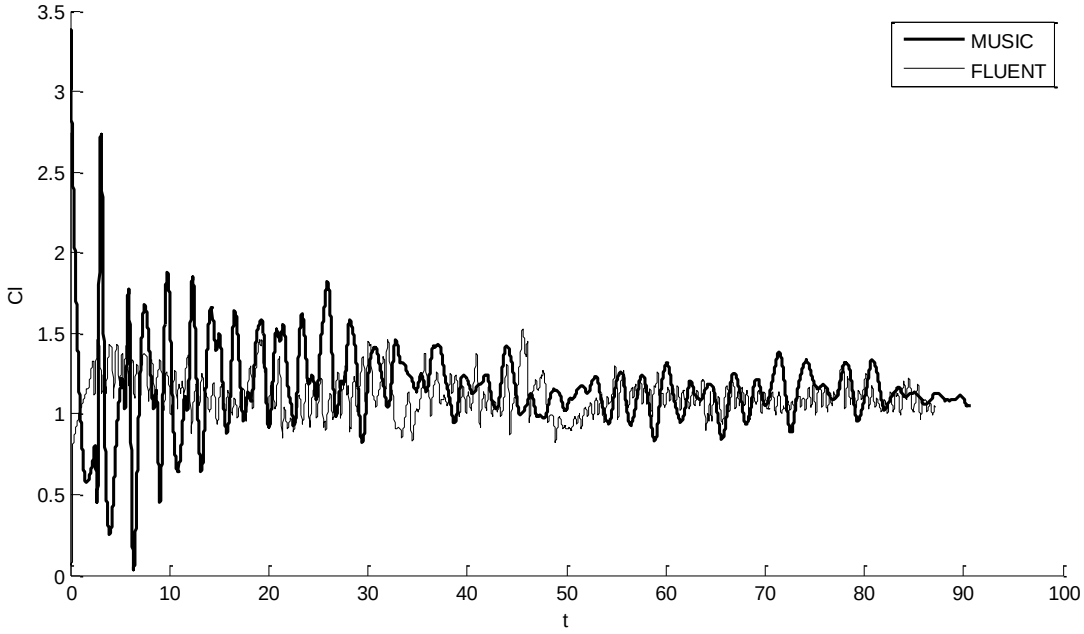

Figure 3-7: Solver verification: lift coefficient history computed by MUSIC and FLUENT

3.1.2 Comparison with the Experimental Results

Using the previously verified numerical methods, the flow around NASA-LS-GW(1) airfoil was simulated under various AOAs, and the result can be seen in Figure 3-8.

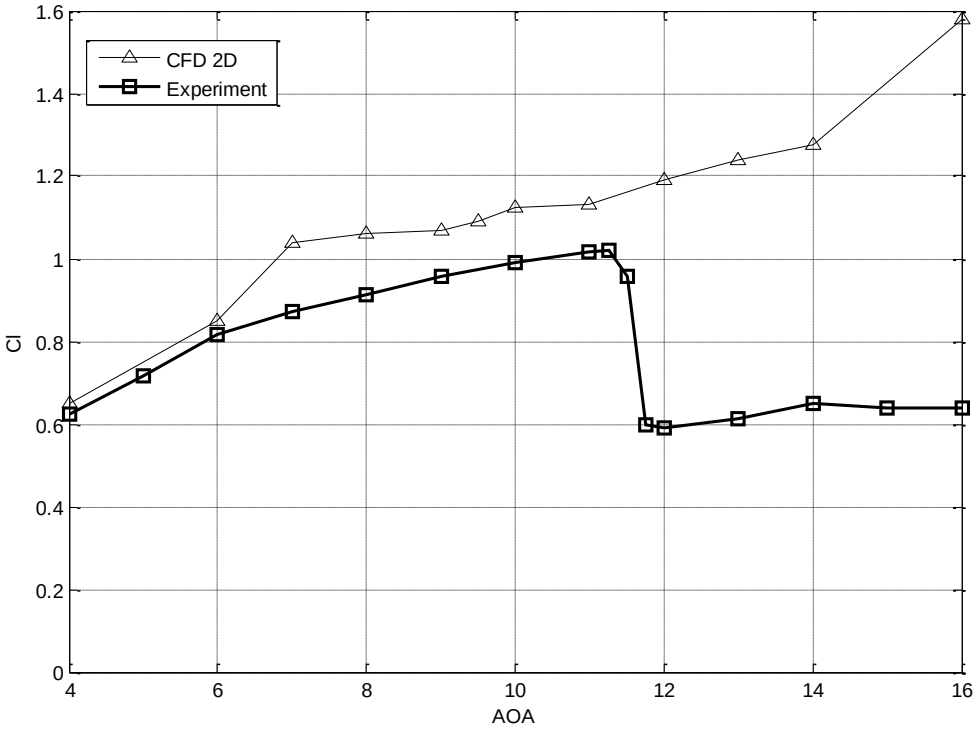

Figure 3-8: Averaged Lift Coefficient: CFD vs. Wind Tunnel Tests

It is obvious that something was not right at post-stall AOAs: instead of stalling behavior, the lift coefficient just kept going up and finally reached more than 200% of the experimental results, the trend was clearly incorrect and unphysical.

Before getting to the post-stall AOAs, attention should first be paid to what seemed to be correct, i.e. the lower AOA cases.

3.1.2.1 The Low-AOA Cases (AOA< 7 deg)

This is the range of AOAs before the transitional separation bubble takes place, the lift coefficient increases with the AOA almost linearly. From the pressure coefficient distribution on upper and lower surfaces at 6 deg AOA (Figure 3-9), it can be seen that the CFD simulation results agreed reasonably well across the whole airfoil section, although the suction peak was slightly lower than that of the experiment. However, when it came to the average flow field (Figure 3-10), the CFD results showed a small separation bubble at x/c≈0.8, and it can be noticed that the pressure distribution is slighted disturbed near that point too. But it is clear that this separation bubble had little, if any, contribution to the overall lift.

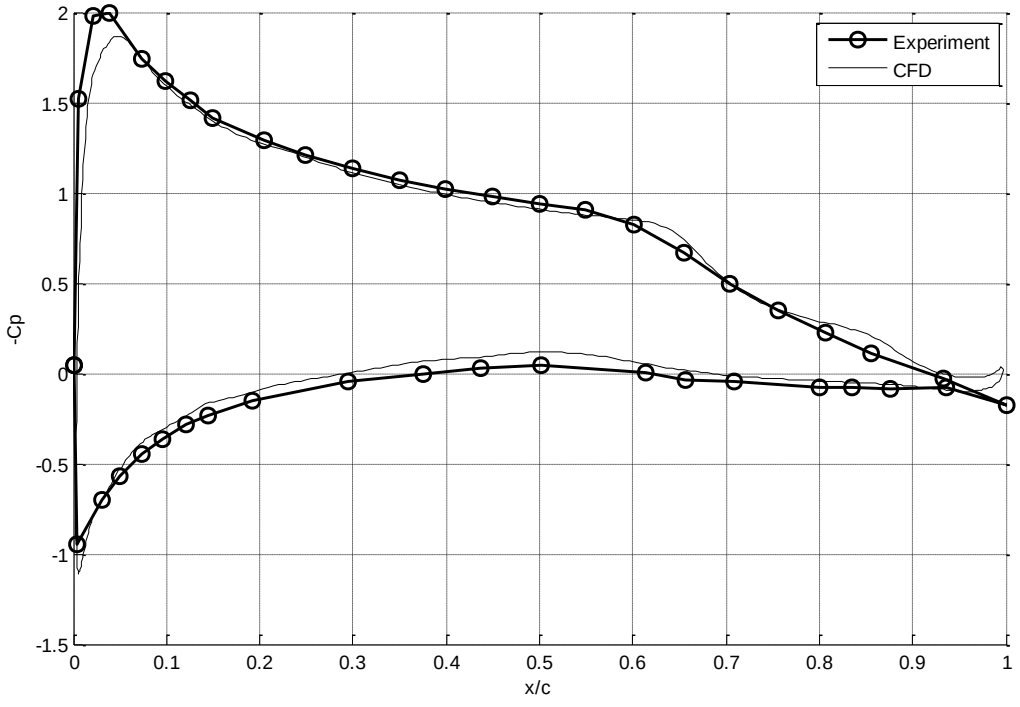

Figure 3-9: Pressure Coefficient Distribution @AOA=6 deg

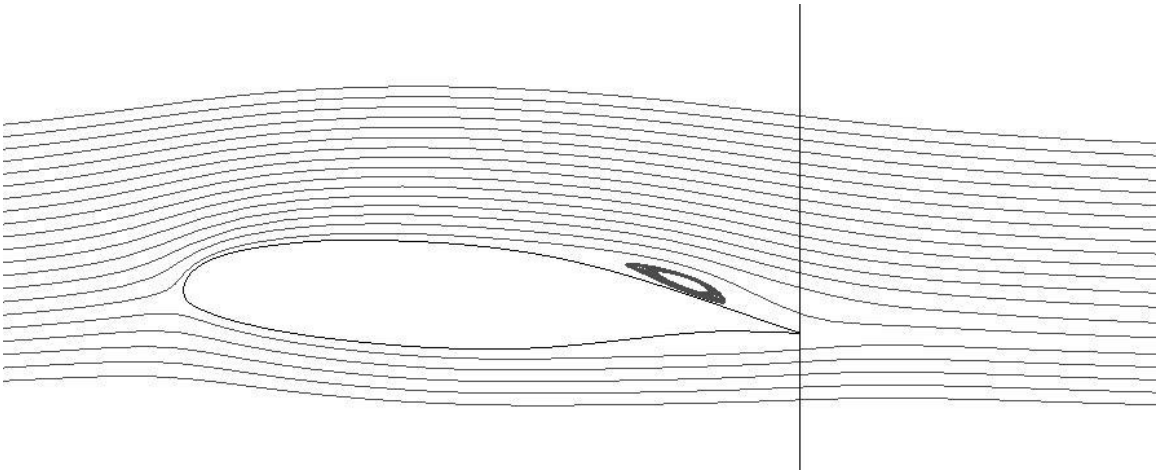

Figure 3-10: Computed Time-averaged Streamline @AOA=6 deg

When the transient flow field was reviewed from Figure 3-11, it showed that the flow, although appeared to be an largely attached flow in the averaged sense, was characterized by a successive vortex shedding behavior, which was confirmed by the PIV measurement, besides, in reference [38], similar behavior was observed on a different airfoil.

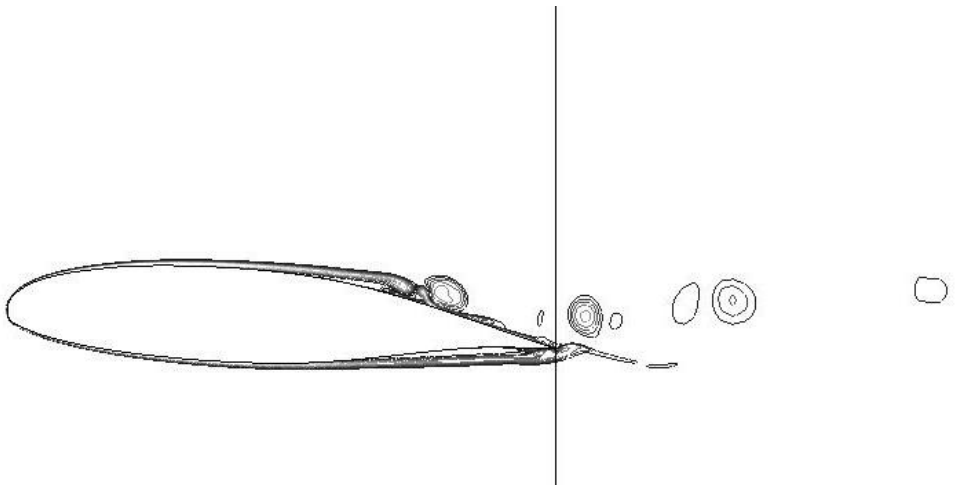

Figure 3-11: Transient Vorticity Contours @AOA=6 deg

3.1.2.2 The Mid-AOA Range (AOA=7-11 deg)

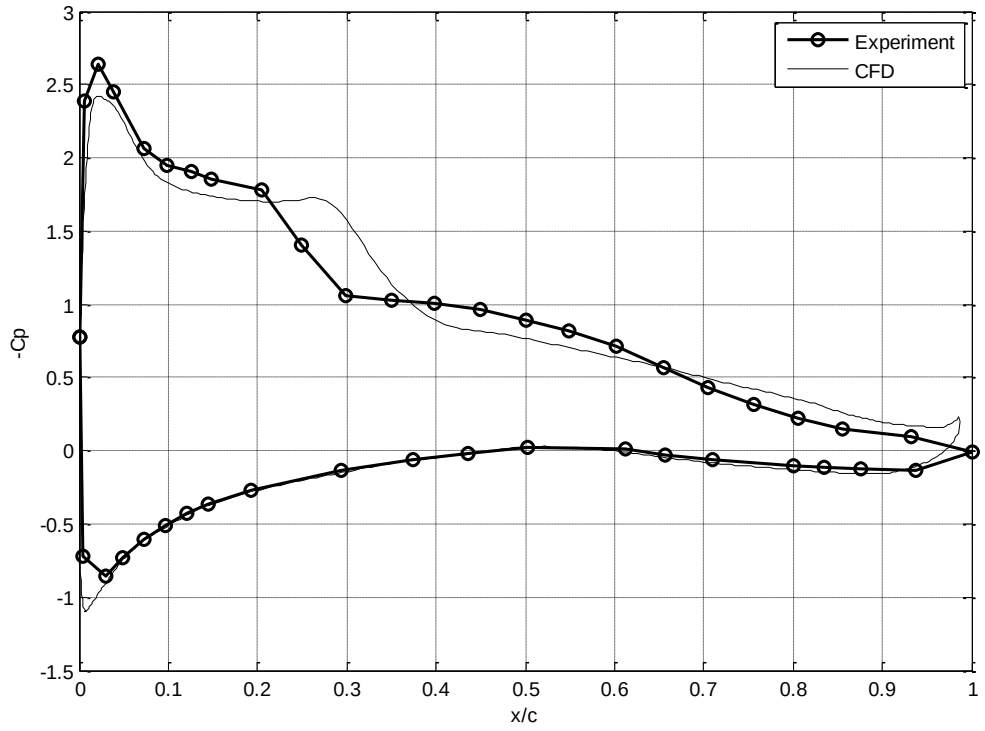

Figure 3-12: Pressure Coefficient Distribution @AOA=9 deg

From Fig. 3-12, the lift coefficients of this region were overestimated. From the pressure distribution, it was clear that the plateau due to the transitional separation bubble was a bit longer than what is measured in the experiment, and this was the source of the extra lift. More precisely, the plateau started at about the same place as the experiment, but the place where the pressure increase position was found to be behind the experimental measurements.

From the average flow field in Fig 3-13, it can be shown that the separation bubble in CFD results tended to be longer, which confirmed the pressure distribution results: the incorrectly predicted position of reattachment is the cause of the error.

In the transient flow field (Figure 3-14), as is pointed out by [15], the so-called separation bubble was also a set of shedding vortex, which took off at some point and landed on the upper surface again somewhere downstream. And this landing place was predicted behind what really was in the experiment.

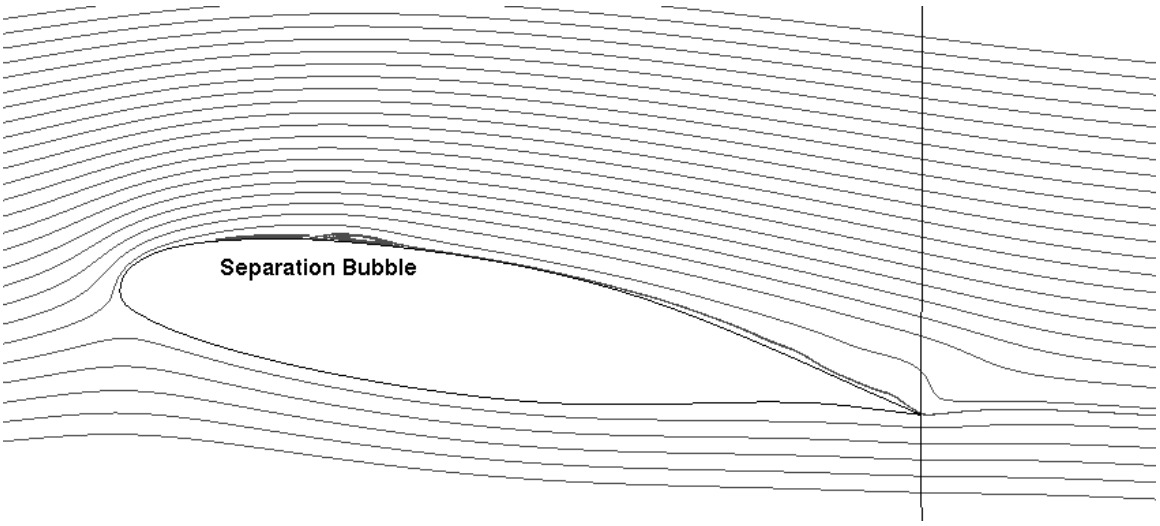

Figure 3-13: Computed Time-averaged Streamline @AOA=9 deg

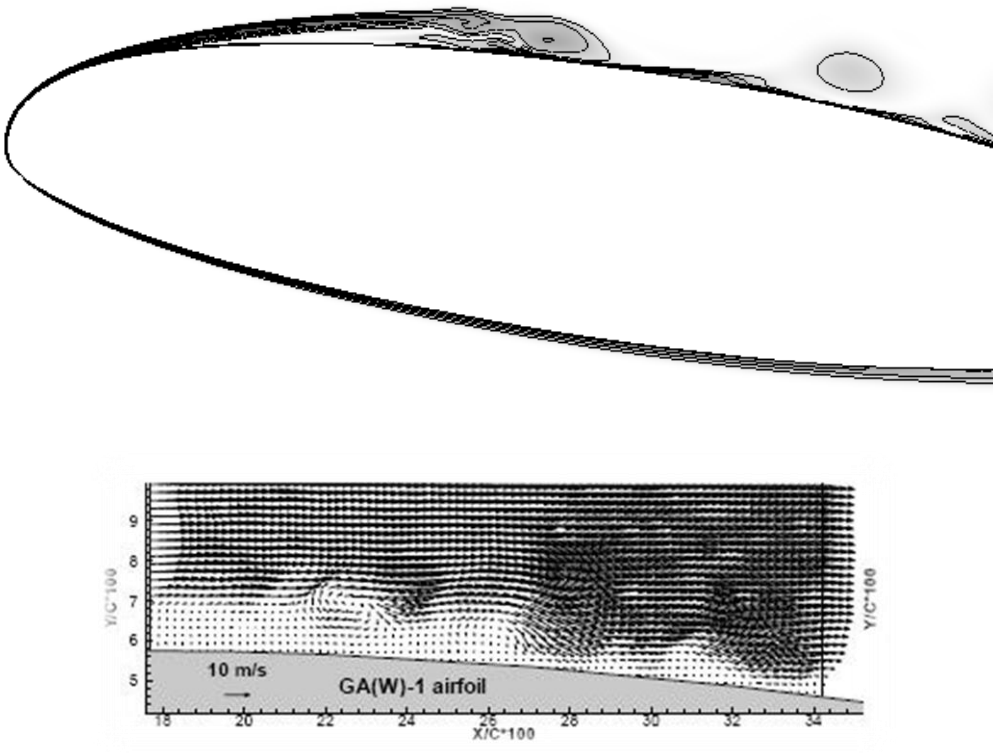

Figure 3-14: Transient Flow Field @AOA=9 deg
Top: Computed Vorticity Contours; Bottom: PIV Measurements

Therefore, all the evidence revealed that it was very likely the 2D N-S equation tended to predict the wrong position of reattachment. Since in low Reynolds number flows, the attachment is very much related to the entrainment of the boundary layer after the transition to turbulence, and it seems that this entrainment was underestimated by the 2D N-S equation. The possible reason for this will be explored in later chapters.

3.1.2.3 Higher AOA Region (AOA>11 deg)

The most interesting part of the simulation was for the post-stall behavior, as can be seen from Fig. 3-8, the trend is obviously incorrect, and it looked as if no stall had ever occurred.

First, in order to make sure the solution was still valid for the high AOA region, verification studies were conducted again and showed quite the same agreement as the 10deg AOA case, as is showed in Fig 3-15.

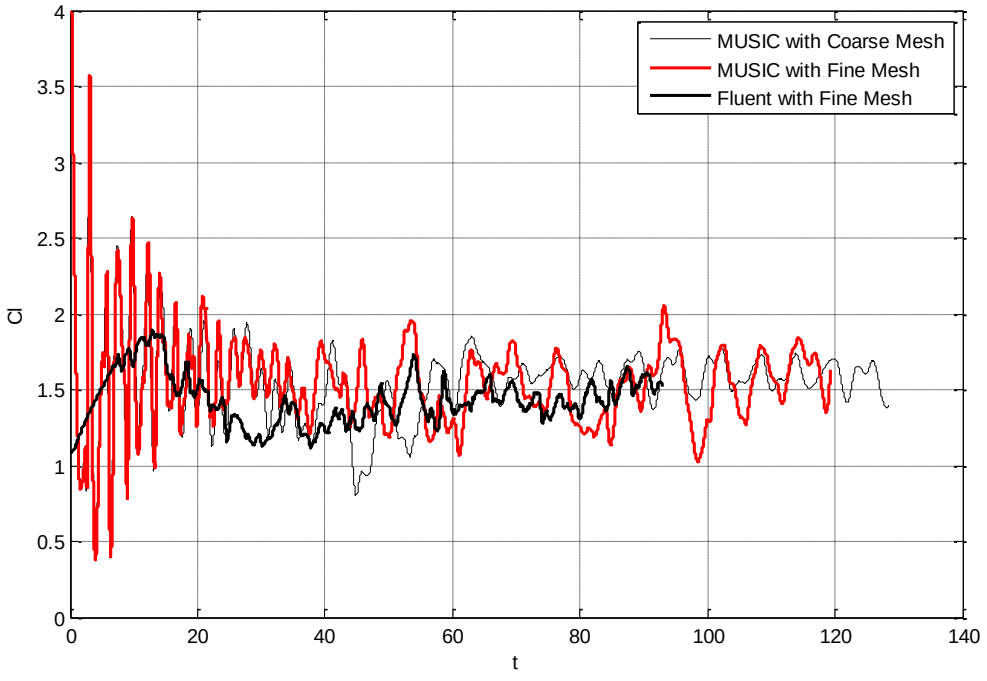

Figure 3-15: Verification of 16deg AOA case with different grids and solvers: Lift coefficient history

Therefore, the solution was believed to be valid, and it was obviously having notable errors when compared to the experimental results (as high as 100% relative error at AOA=16 deg). Then the flow field by the CFD was looked over and compared to the PIV measurements.

The result of the time-average showed considerably difference: it was found that the computed flow field actually did not stall! Since from Fig. 3-16, we can still see the separation bubble and reattachment, although the bubble had grown to be much thicker than AOA=10 deg case, and was seemingly composed of more than one vortex structures. However, in the experimental result from AOA=15, a very big recirculation zone was already generated above the airfoil, and the airfoil had completely stalled (Figure 3-17).

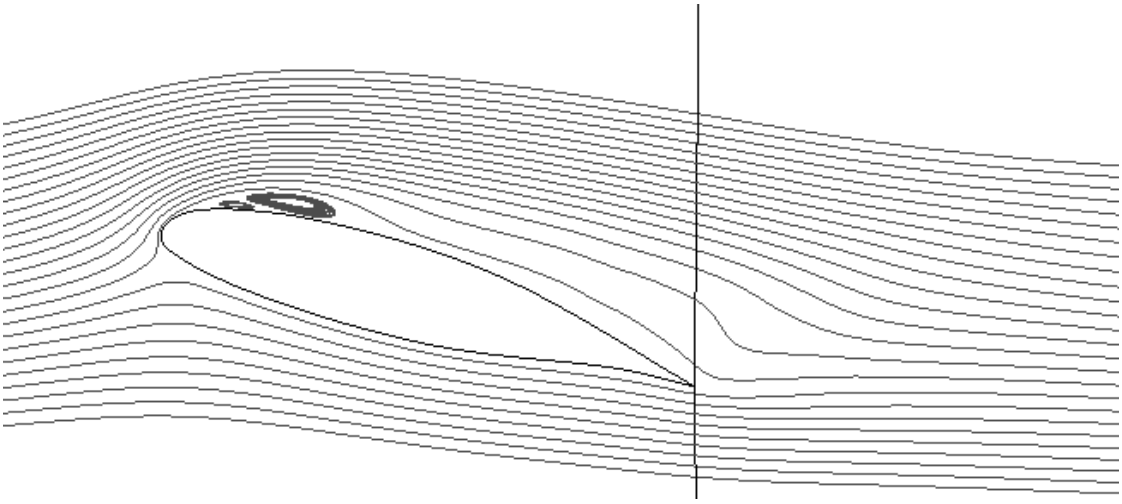

Figure 3-16: Computed Time-averaged Streamline @AOA=16 deg

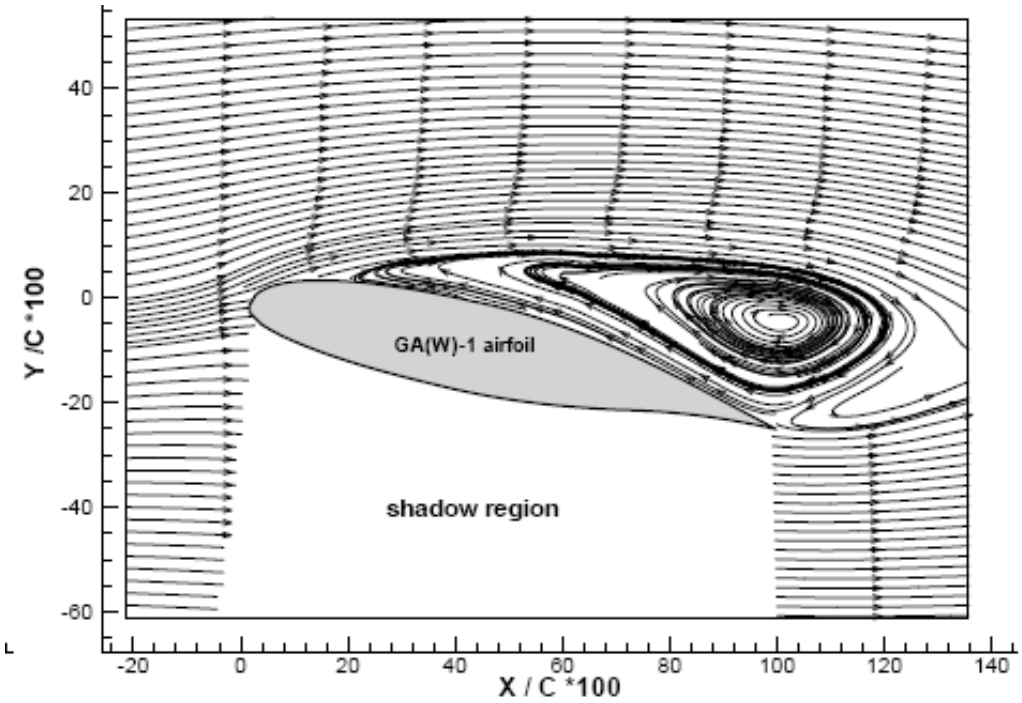

Figure 3-17: PIV measured flow field @AOA=15deg [15]

This observation was confirmed by the CFD result of the pressure distribution, as can be seen from Fig 3-18, it was very similar to the mid-AOA cases, with an apparent

separation bubble, and the suction peak near the leading edge remained intact, and with even higher pressure difference. However, in PIV measurement, the suction peak had already collapsed due to the big low speed zone created by the big circulation above the airfoil.

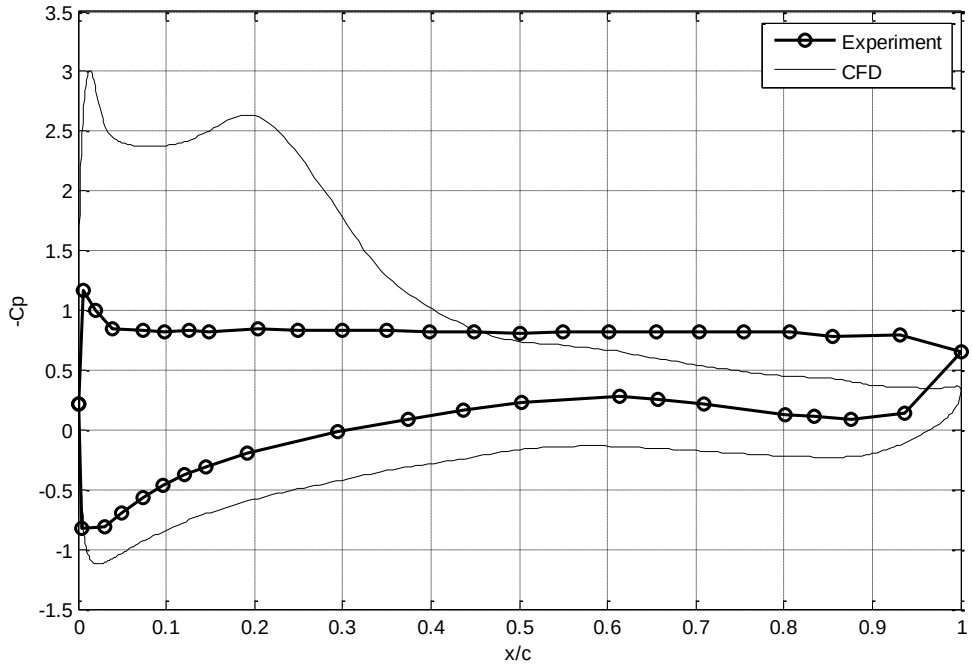

Figure 3-18: Computed pressure coefficient distribution @AOA=16 deg

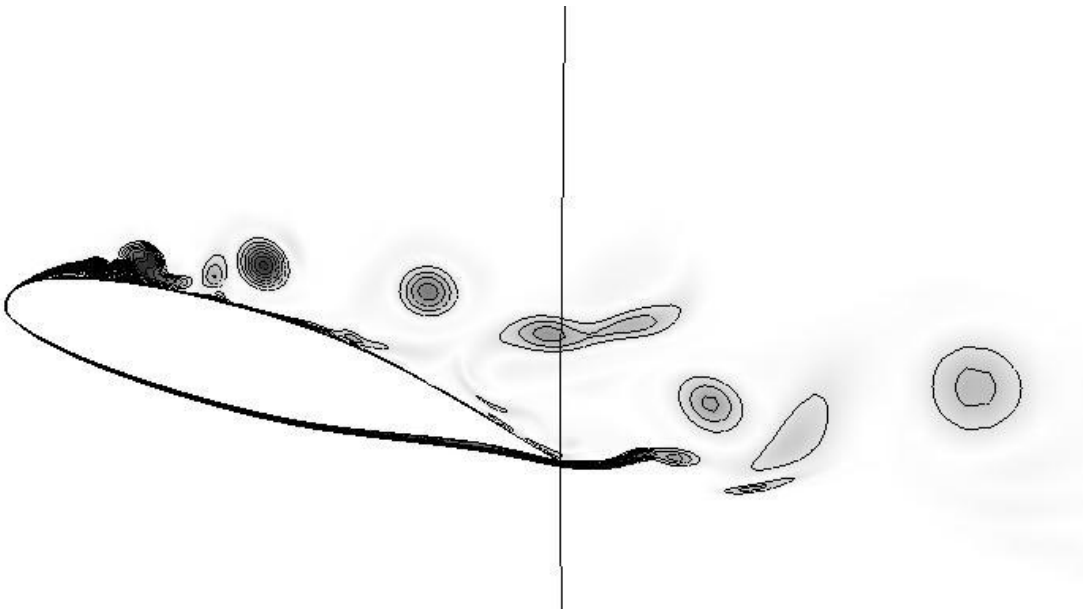

Figure 3-19: Computed Transient Vorticity Contours

And for the transient flow field, what happened in the experiment was that the shedding vortices took off near the leading edge and never landed on the surface again, while in the CFD measurement, the vortex took off at quite the same place, but it was still kept close to the upper surface, and the suction peak was retained.

Shortly put, for high AOA region, 2D Navier-Stokes solution was unable to predict the burst of the separation bubble, and the collapse of the suction peak, and thus the whole stall behavior was missing.

3.1.3 Discussion of the 2D Navier-Stokes Solution

Well-designed numerical tests were performed to eliminate various types of errors, but large errors still came out of the high AOA cases. So did this error come from 2D Navier-Stokes equation itself or anything else?

It was also reasonable to consider the missing smaller scale turbulence motions since all the tests were conducted without using any turbulence model. However, if this big error was indeed caused by the small scale fluctuations, refining the mesh should surely help considerably reduce the error. But the grid refinement study showed little difference.

Therefore, unless some unknown error source, which was potential of causing 100% error, was responsible for the incorrect results, the error was very likely to come from the 2D Navier-Stokes equation itself. To confirm this, a 3D simulation is definitely necessary.

3.2 3D simulations

For the results from 3D simulation to be valid, a series of numerical verification study would be needed. However, because of the limitation of computing power, it was impossible to do the grid refinement study as thoroughly as what is done for 2D. Therefore, the point of the 3D simulation in the present study was to uncover the 3D effects on a 2D airfoil computation with as much resolution as was made possible by the resources at hand.

The 3D mesh was created by an extension of the coarse 2D grid, and several cases were tested to verify that the computational domain size and the grid resolution in the spanwise direction would not cause significant numerical uncertainties. And after a series of comparison, finally the computational domain size was chosen as one chord length spanwise, and a balance of reasonable and affordable mesh size (320×80×40) was chosen to perform the computation, which is far less than LES/DNS required resolution.

Boundary conditions were the same as those in 2D simulation with the addition of the front and back symmetry boundaries.

3.2.1 The Case for AOA=16 deg

The most evident disagreement of 2D results with experimental ones happened in the post-stall region, where the 2D CFD was not able to capture the large separation zone in the average flow and thus cannot predict the drop of the lift coefficient.

From the lift coefficient history (Fig 3-20), 2D and 3D result showed clear differences: in the beginning phase, C_L by 2D and 3D simulations were very similar, by after some time, the 2D and 3D simulation developed quite differently, with the 3D simulation slowly approaching the experimental results.

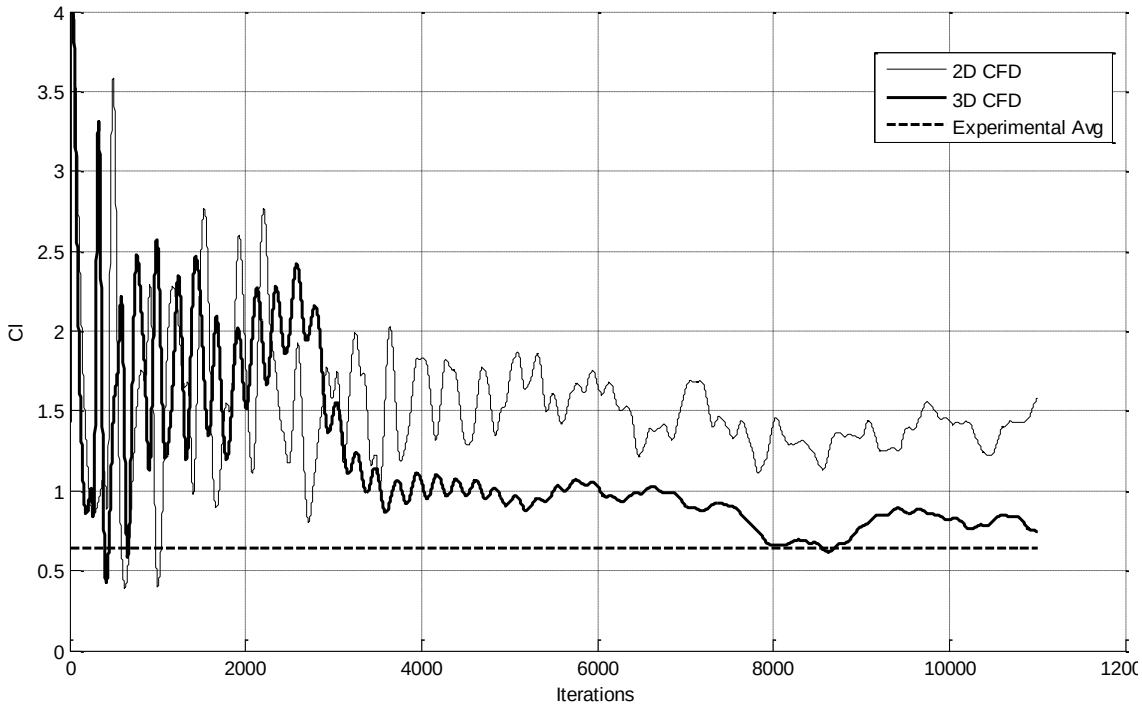

Figure 3-20: Lift Coefficient History, 2D CFD vs. 3D CFD

And in terms of the time-averaged flow fields (Fig 3-21), the large circulation zone was clearly revealed by the 3D simulation, which was very close to the PIV measurements, in both the position of the dominant recirculation center and the position of the smaller vortex. From the transient vorticity iso-surface colored by Mach number in Fig. 3-22, it can be seen that the flow was completely three-dimensional, with large variations in the third dimension. It should be noted that no disturbance was added to the initial condition

in all the 3D simulations, which means that all the 3D structures developed out of numerical truncation errors of the implicit time marching.

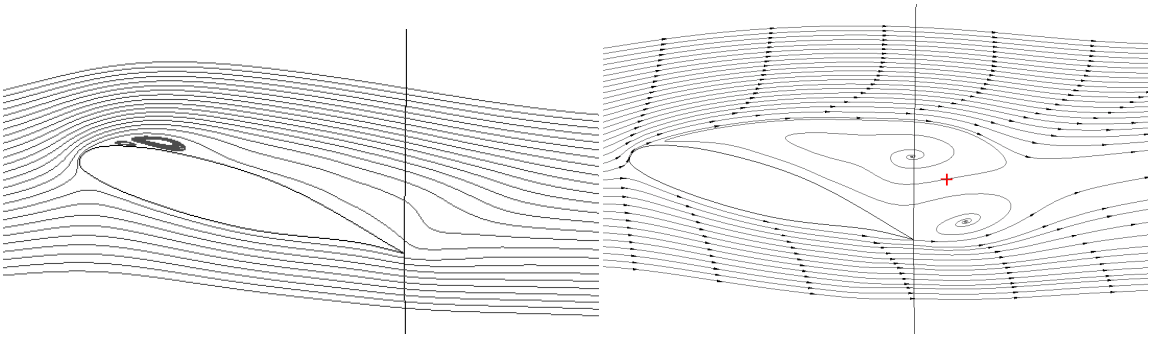

(a).2D (b). 3D

Figure 3-21: Computed Time-averaged Streamline @16deg AOA

Therefore, there was no doubt that 3D simulations, even with a relatively coarse grid, yielded completely different results both in flow structure and aerodynamic performance, and the 3D result was apparently closer to the experimental result and made much more sense in terms of post-stall behavior.

And then, 3D simulations were performed for other AOAs, to see what trend of the lift coefficients would be revealed compared to 2D simulations.

Figure 3-22: Transient Vorticity Iso-surface colored by Mach number

3.2.2 Flow Simulation for Other AOAs

Flows with a range of AOAs from separation bubble range to post-stall range were simulated, and the results of lift coefficients are shown below in Fig. 3-23. An abrupt drop of lift can be observed, which agrees with the leading edge separation feature, however, the stall happened at an AOA that was one degree smaller than it did in the experiment. Besides, when compared with 2D simulation results from fine grid, it only showed conspicuous difference after the stall. It can be seen that 3D simulation results were not perfect even in the higher AOA range, but it is fairly encouraging to see the lift drop due to the stall behavior. The discrepancies of 3D simulation were probably due to the limited mesh resolutions.

When combining 2D and 3D simulation, a lift coefficient curve versus AOA can be drawn. For lower AOAs for mainly attached flow, 2D simulation can provide a good estimation in the low AOA region, while for the mid range AOAs, where the separation bubble plays a part, there was up to 20% overestimation of C_L, both for 2D and 3D simulations. An early stall and about 20% overestimation were obtained by 3D simulation in the post-stall region, while 2D simulation got a completely wrong trend here.

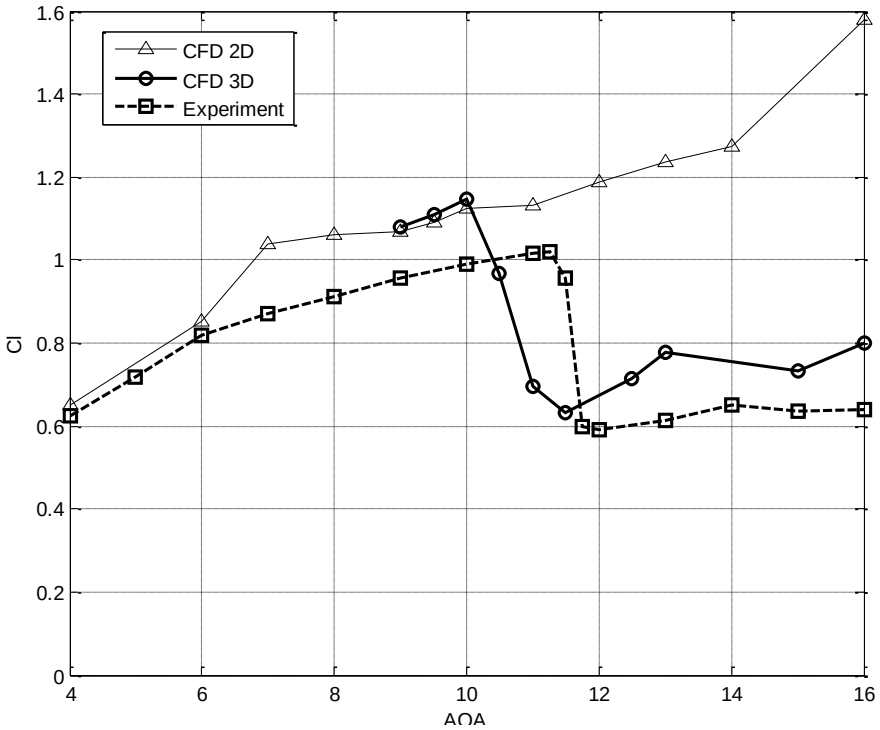

Figure 3-23: Lift coefficients, CFD vs. Experiment, CFD computed by 2D and 3D simulation

These results presented in Figure 3-23 suggests that the incapability of 2D Simulation in the post-stall AOAs, because the large separation zone in time-averaged flow field never happened, and however the AOA increased (up to 20), the result from a 2D simulation would still be averaged to a separation bubble flow field, with a much higher suction peak.

As is analyzed in previous chapters, the considerably large error from 2D simulation should come from nothing but 2D Navier-Stokes equations, and this was confirmed by the 3D CFD simulations. But there was still more to explore: Why exactly is a 2D simulation incapable of producing the stall? And how can the error in the range with AOA from 8-11 be explained? An explanation needs to be proposed from simulation results obtained.

3.3 Discussion of Numerical Results of the Smooth Airfoil

3.3.1 An Unsteady Perspective of the Flow Field

Traditionally, researchers tended to look at flow fields with the assumption that the flow was steady, just as in the all the studies on separation bubbles and the big vortex structure in a stalling airfoil flow field, and people have developed a whole theory in order to recognize the vortex structures based on topology and surface oil flow experimental results [42].

However, at least in the low Reynolds number regime, the flow usually appears to be composed of much more than several static vortices in almost fixed positions, but with a set of large scale unsteady vortex motions, which was revealed by both experimental studies by Hu and Yang (2007) [15] and the current study. As can be seen from Fig 3-24, even in a flow with AOA=0 deg, there was large scale vortex shedding near the trailing edge.

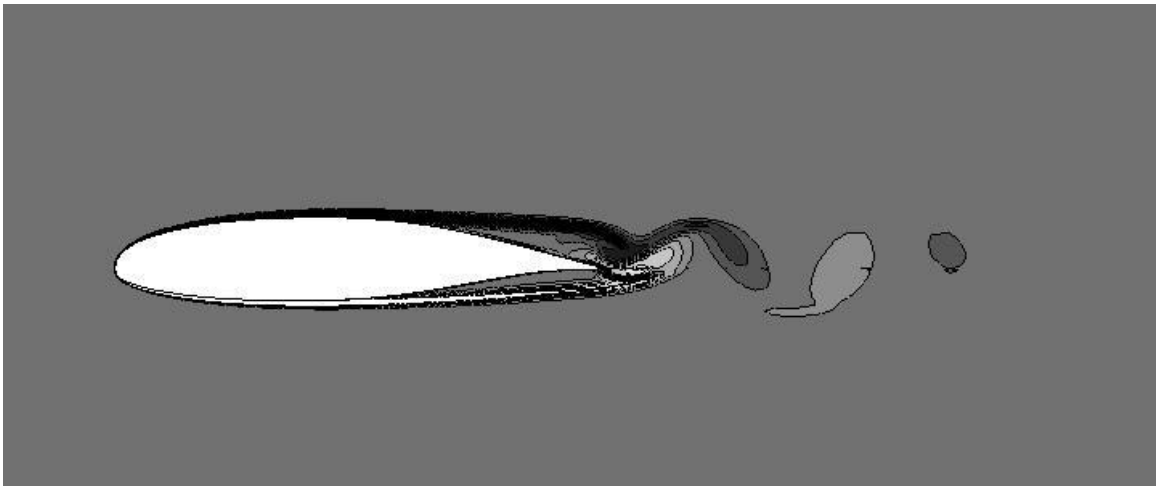

Figure 3-24: Computed Unsteady Vortex Motion @AOA= 0deg

The unsteady nature of the flow field reveals that the previous studies on separation bubbles and steady separation structures at this Reynolds number were virtually nothing more than the time-averaged aspect of the flow field. This would also mean that in an actual flow field of this Reynolds number, structures such as a separation bubble never really exist.

Therefore, the question would come up what are the corresponding transient structures for those mean flow structures people are familiar with for this Reynolds number. And reference [15] has already explored this issue. For attached flow, the transient counterpart was successive vortex shedding near the surface; for separation flow, the transient behavior was that the vortex sheet "took off" from the surface and "landed" again; as for post-stall flow with large separation, the transient counterpart was that the shed vortices went away from airfoil surface. Inferred from these test results, the stall, or the form of large separation structures, was virtually a change of path along which the vortices shed.

And the cause of the stall, first would be related to increase the adverse pressure gradient on the upper surface as the AOA increases, and secondly, would be related to 3D structures, based on the result of previous two chapters that a 2D Navier-Stokes simulation was unable to predict the stall behavior.

3.3.2 3D Effects in Quasi-two-dimensional Flows

It is widely believed that Quasi-two-dimensional flows are unstable to 3D perturbations, but not much is known about how the instability is developed. The centrifugal instability of a circular symmetric flow was studied by Rayleigh (1916) [43] for the inviscid case and Taylor (1923) [44] for the viscous case, and Bayly (1988) [45] extended the study to a class of inviscid closed-streamline flows, and in [46], he also studied the 3D instabilities of elliptical flows, which suggested a mechanism by which 3D complex flows can arise from large-scale two dimensional coherent structures first discovered by Pierrehumbert (1986). And these studies, although mostly about inviscid flows, should still be enough to suggest that the instability of a quasi-2D flow at relatively high Reynolds numbers. Therefore, it is very easy for a disturbance in the spanwise direction to grow and finally cause the whole flow field to become 3D.

And the results from the present study also showed evident instability in the third dimension for this quasi-2D flow (Fig 4-3), and the resulted 3D flows showed significant differences from their two dimensional counterparts. So it is clear that the flow will be 3D instead of 2D for such Reynolds number due to the instability, and the next thing, we should look at the differences caused by the 3D structures more closely.

The most striking difference, as can be seen from the previous chapters, was in the flow of post-stall AOAs, in which it seemed that only a 3D simulation was capable of producing the large separation zone above the airfoil, and thus predicting the right trend of the lift.

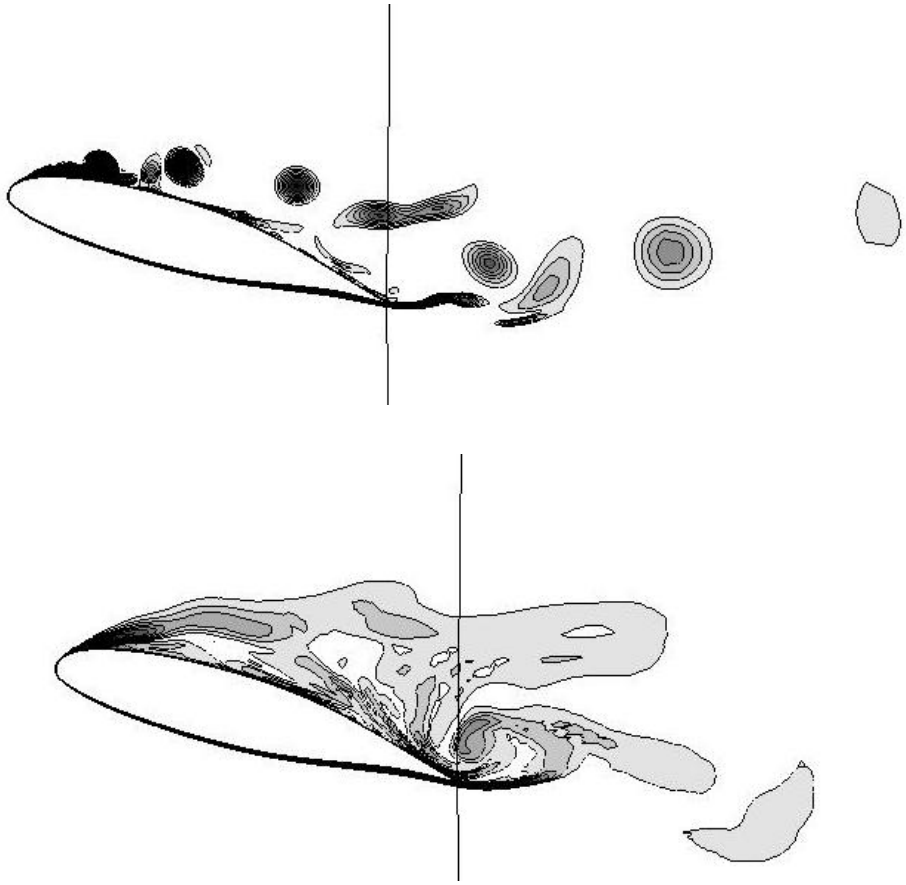

Figure 3-25: Comparison of transient vorticity contours by 2D (top) simulation and 3D (bottom) simulation (median-span plane) @AOA=16 deg

To explore the reason for the considerable difference, the transient flow fields at AOA= 16 deg needed to be looked at more closely (Fig 3-25). In the figure below, the vorticity contours from the 2D simulation and the median-span plane of the 3D simulation were compared, and obvious disparity can be observed. In the result from two-dimensional simulation, the vorticity was concentrated and located in a few very large vortex structures, and these large-scale vortices propagated in a path that is very close to the upper surface. Whereas in the computed transient vorticity distribution from the 3D simulation, concentrated vorticity only existed near the leading edge, or the separation point, after that, the voticity is spread in the whole region above the airfoil and no concentrated vortices were present.

The above observation seemed to suggest that the diffusion of the vorticity is completely different for 2D and 3D simulations. Explanation can be easily found from vorticity transport equations (incompressible) below:

$$\frac{\partial \omega_i}{\partial t} + \left(u_j \frac{\partial}{\partial x_j} \right) \omega_i = \left(\omega_j \frac{\partial}{\partial x_j} \right) u_i + \nu \nabla^2 \omega_i$$

For 2D Navier-Stokes simulation, only one of the 3 equations above is valid, while in a 3D simulation, all the three equations are valid. And the diffusion term $\nu \nabla^2 \omega_i$ on the right hand side also triples when switching from 2D to 3D, which means vorticity can diffuse in all the three directions. In a 3D flow field, large vortices would be distorted and even intertwined by the growing three-dimensional disturbance, and would then easily break down to smaller scale structures in all the directions and be finally diffused to the whole region. This process also delivers the energy to the smaller scale motions, and finally causes the transition to turbulence. However, in a 2D Navier-Stokes simulation, the vorticity is "trapped" in those 2D large vortices structures, and the diffusion of vorticity only happens around those vortices, which prevents the vorticity from being diffused to a large region and also prevents energy from transporting to smaller scale eddies.

For post-stall AOAs, vorticity was concentrated in large vortices in 2D simulation, the propagation of which formed a high speed flow area (Fig. 3-26), which allows the pressure to build up from the trailing edge, and thus the suction peak near the leading edge was retained. However, in a 3D simulation, which was closer to the real flow, the vorticity was diffused, along with the energy. With lots of energy in the spectrum of smaller scale eddies, a large low time-averaged speed region was formed instead of a high-speed region, and within this low speed region, the pressure would stay almost the same, which impeded the pressure build up from the trailing edge, and thus caused the collapse of the suction peak, as is demonstrated in Fig. 3-27 and Fig. 3-28.

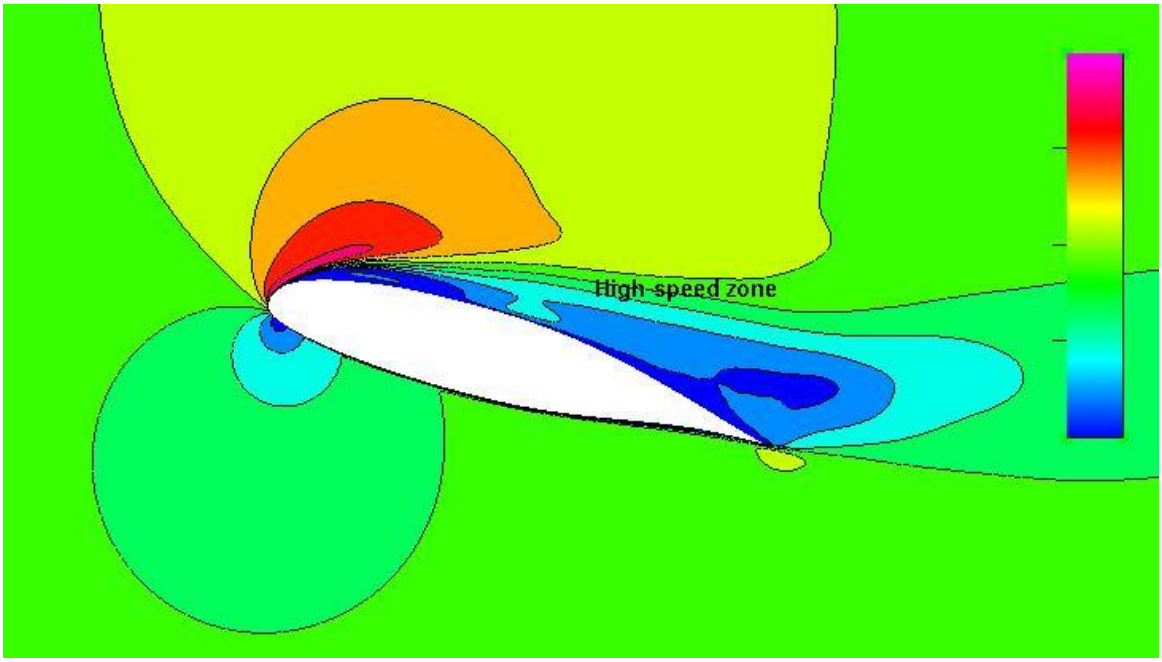

Figure 3-26: Time-averaged velocity contours from 2D simulation

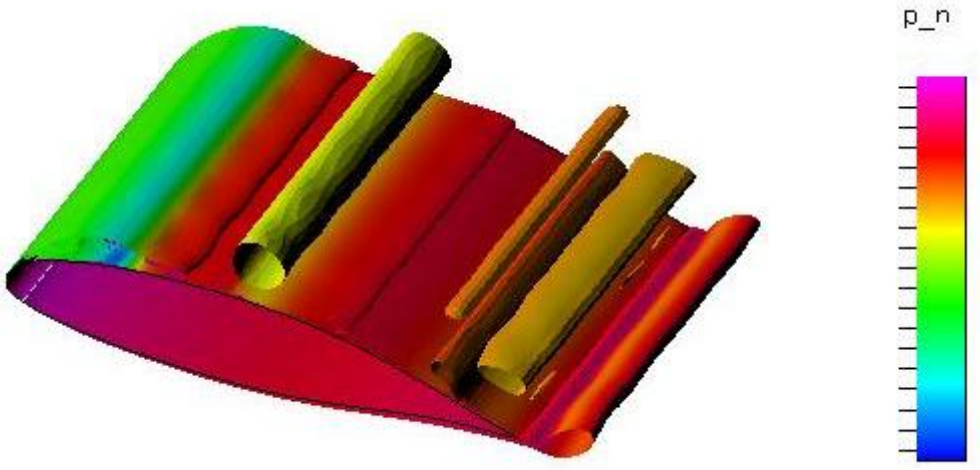

Figure 3-27: Vorticity iso-surface colored by gauge pressure @AOA=16 deg, before 3D structures developed, the vorticity was concentrated in large scale motions and a low pressure region (suction peak) near the leading edge on upper surface was retained.

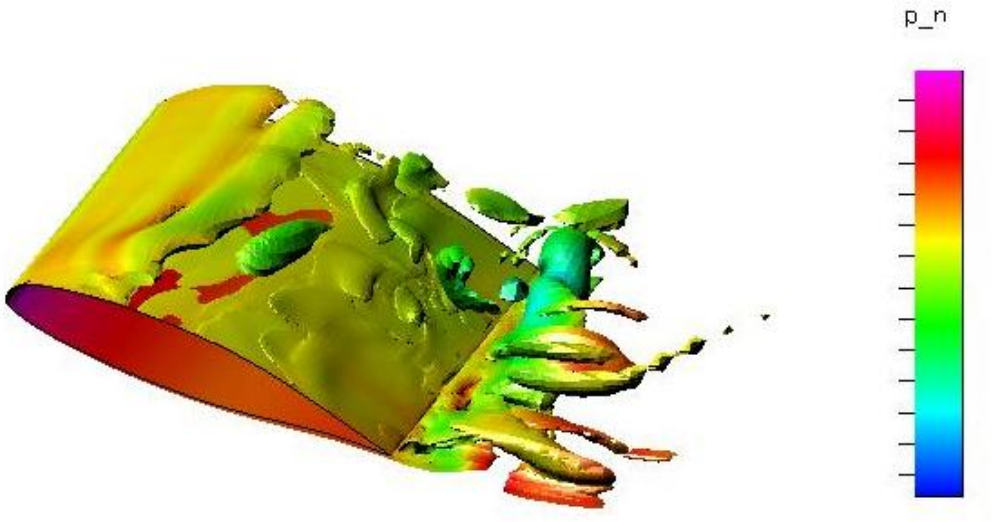

Figure 3-28: Vorticity iso-surface colored by gauge pressure @AOA=16 deg, after 3D structures fully developed, vorticity was diffused into smaller scale motions across a large area and the suction peak near the leading edge has collapsed.

Therefore, from this study, it seems that the stall of an airfoil is closely related to the development of large scale 3D structures, especially the role these structures play in the diffusion of vorticity, and a 2D Navier-Stokes simulation appears unable to predict the right physics in post-stall AOAs.

The fact that 2D and 3D simulation yielded similar results at lower AOAs does not necessarily mean that these flow fields are mainly two dimensional (Figure 3-29, 3-30). In the experiment, what actually happened was that before the airfoil stalled, the shed vortices propagated near the surface, which means they are somewhat “trapped” in the boundary layer too. And a 2D simulation, although unable to describe the 3D structures, is able to describe flow with the vortices propagating along the surface. This can be demonstrated with Fig. 3-29, which shows the transient flow field of a lower AOA case: although the flow is clearly 3D, the vorticity is mostly concentrated near the surface.

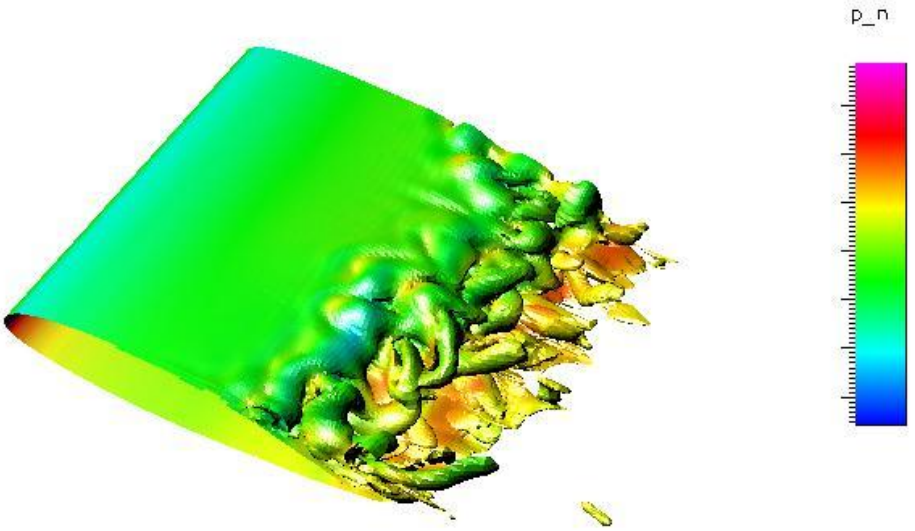

Figure 3-29: Vorticity iso-surface colored by gauge pressure @AOA=4 deg: the flow was 3D, but most vorticity was contained near the surface.

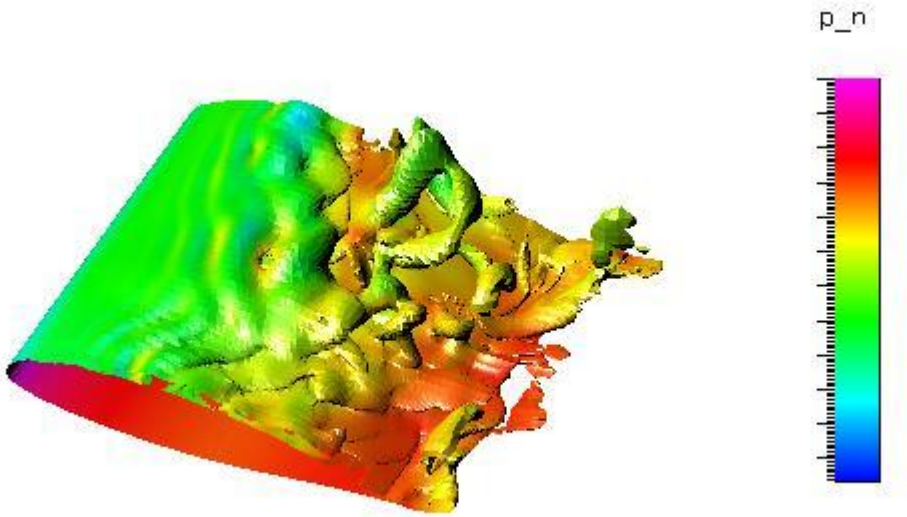

Figure 3-30: Vorticity iso-surface colored by gauge pressure @AOA=10 deg, vorticity was mostly concentrated near the surface, and the suction peak was retained.

However, difference can still be noticed, as in Fig. 3-10, the 2D simulation showed a small separation bubble that appeared not present in the experimental result, which could be possibly due to the fact that the vortices predicted by a 2D simulation were still more concentrated than they really should be.

Another result that needs noticing is that at middle-ranged AOAs, both 2D and 3D overpredicted the lift. A closer look at the simulated flow field revealed that in both 2D and 3D cases, the predicted reattachment positions were farther downstream than what was shown in PIV measurement. The reattachment is usually associated with the energy entrainment of smaller scale eddies. For the 2D case, the solution was almost grid-independent according to Chapter 3, and it cannot produce the smaller scale eddies needed to facilitate the reattachment due to insufficient diffusion by 2D N-S equation. Whereas for the 3D case, it was the lack of grid resolution that caused the dissipation of smaller scale eddies, since it was not a grid-independent solution. The earlier stall predicted by 3D simulation was also caused by the insufficient resolution. If the 3D mesh could be refined to resolve smaller scale eddies, better agreement with the experimental data would be expected.

Chapter 4

The Numerical Simulation of a Corrugated Dragonfly Airfoil

In this chapter, the same strategy used on a smooth airfoil was used on a corrugated dragonfly airfoil. First, a systematic verification study was conducted to minimize the numerical uncertainties in a 2D base case simulation, and then with the proper simulation parameters, the 2D simulation was performed for other AOAs. After that, 3D simulation was conducted for some AOA where 2D simulation had trouble.

4.1 Airfoil Geometry and Meshes

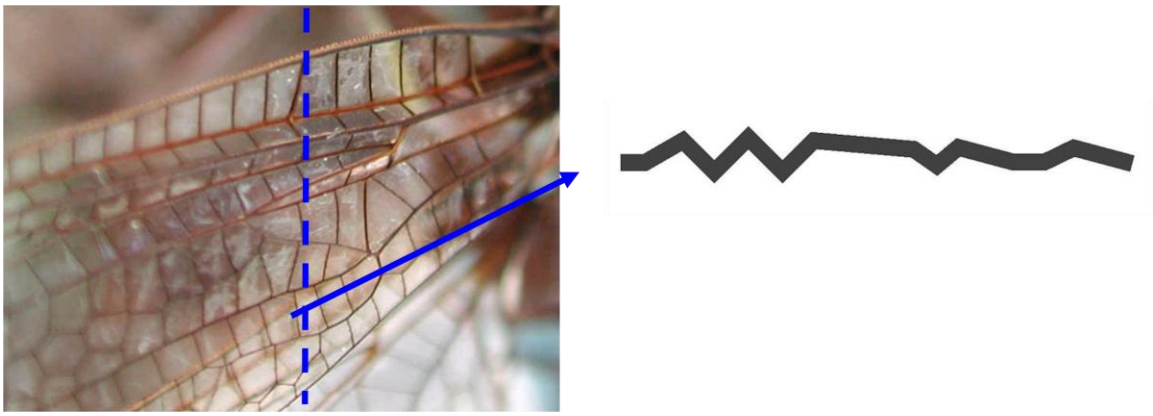

Figure 4-1 the geometry of the dragonfly airfoil

The corrugated profile of the airfoil under investigation is based on a real wing dragonfly (Figure 4-1); it is found that this kind of the geometry can obtain superior aerodynamic performance even without any flapping motion [47]. The reference experimental data of this airfoil was obtained at Reynolds number 55,000.

For current study, two different meshes were used: a coarse mesh of 64408 cells (Figure 4-2a) and a fine mesh of 200208 cells (Figure 4-2b), a multi-block structure type grid was used with necessary clustering at the corners of the airfoil.

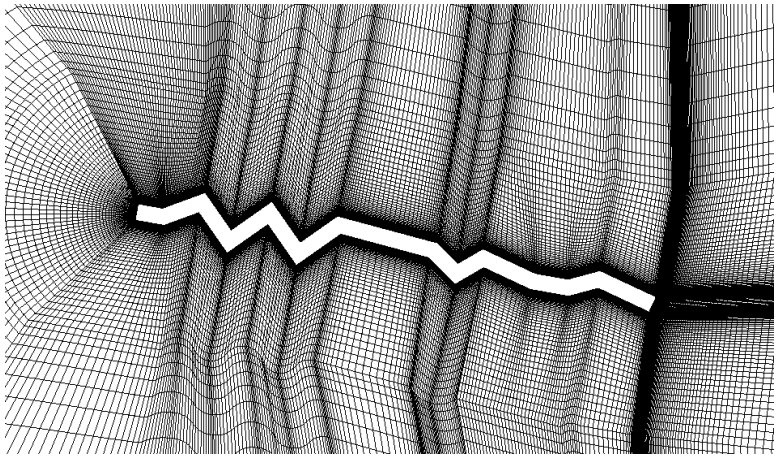

(a)

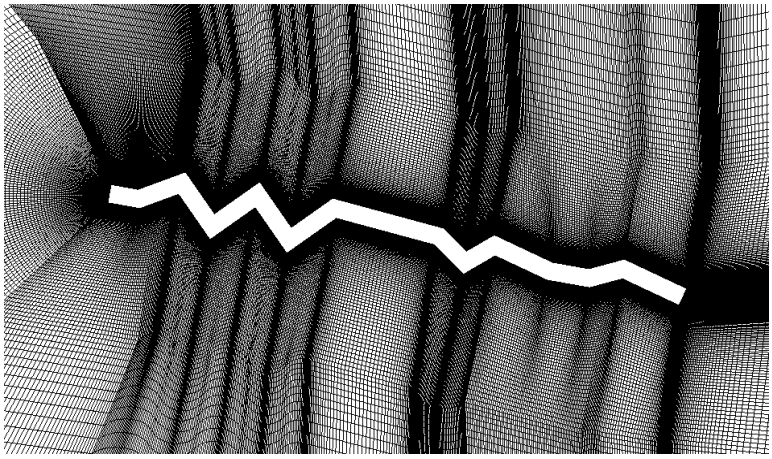

(b)

Figure 4-2 Coarse (a) and Fine (b) meshes of dragonfly airfoil

4.2 Numerical Verification Study

To test the validity of 2D simulation on this unconventional airfoil, it is also necessary to eliminate or at least minimize the numerical uncertainties from different factors. The same types of numerical verification studies were performed just as what were done for the smooth airfoil. For example, the Figure 4-3 and Figure 4-4 below show the grid refinement study and solver verification of the base case, which was also chosen to be the case of AOA = 10deg. This time, the verification solver was a 3rd order spectral difference solver. The mesh for the 3rd order solver was coarser, but with similar number of degrees of freedom as the mesh used for finite volume solver. Similar comparisons were also made for domain sizes, boundary condition types, time steps and inner iteration convergence criteria too.

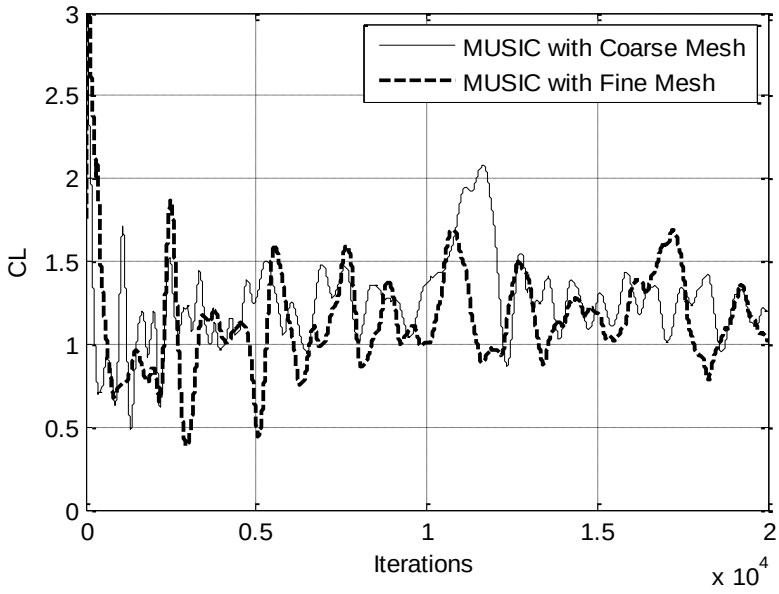

Figure 4-3 The lift coefficient history computed by MUSIC with coarse and fine meshes

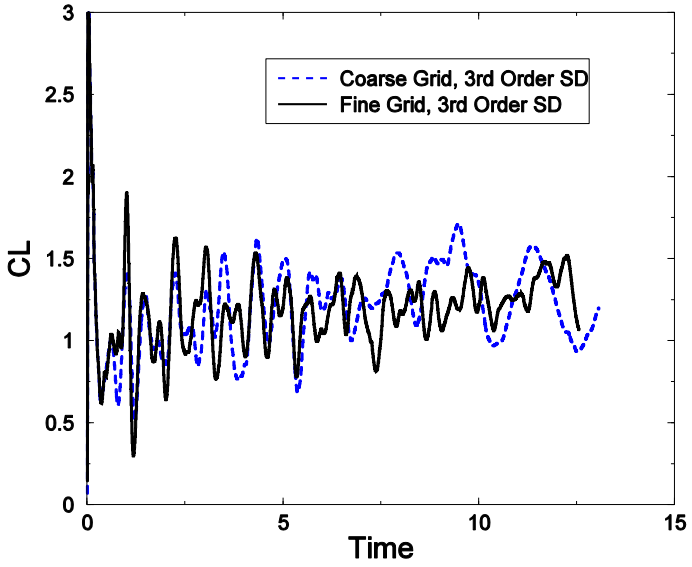

Figure 4-4 The lift coefficient history computed by 3rd order spectral difference solver with coarse and fine meshes

Another factor to consider is the presence of sharp corners in the geometry, since ideal sharp corners do not really exist in real life and it may be able to cause numerical singularities which can also be a source of numerical uncertainties. Therefore, another version of geometry was created with blunt corners instead of sharp corners (Figure 4-5), and then with the same grid resolution, the result was compared to the sharp corner version, which showed almost no difference in both statistics and transient history of lift coefficients.

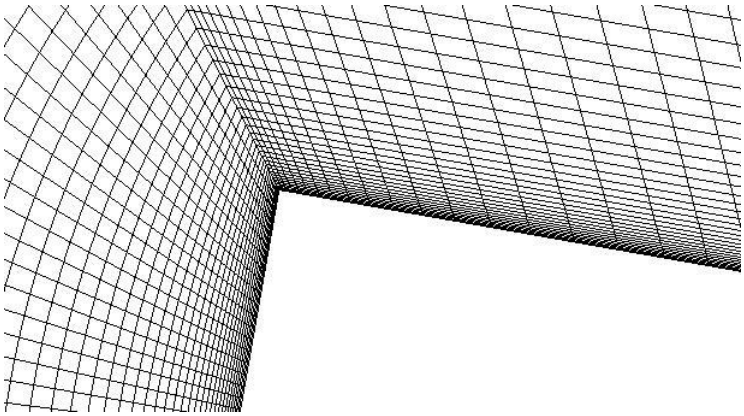

(a) Original sharp corner geometry

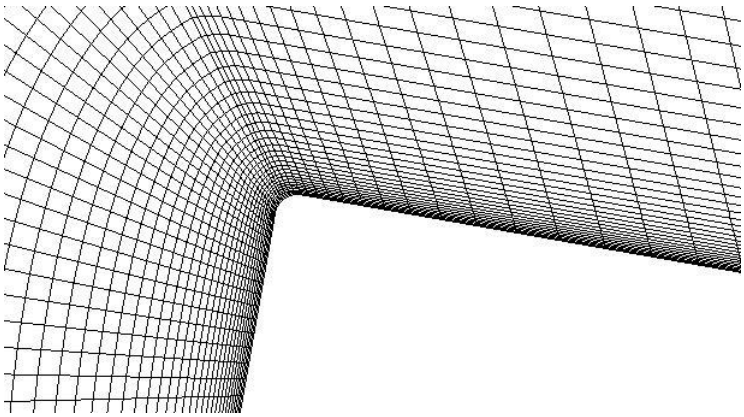

(b) Modified blunt corner geometry

Figure 4-5 Geometry modification for testing the numerical uncertainty by ideal sharp corners

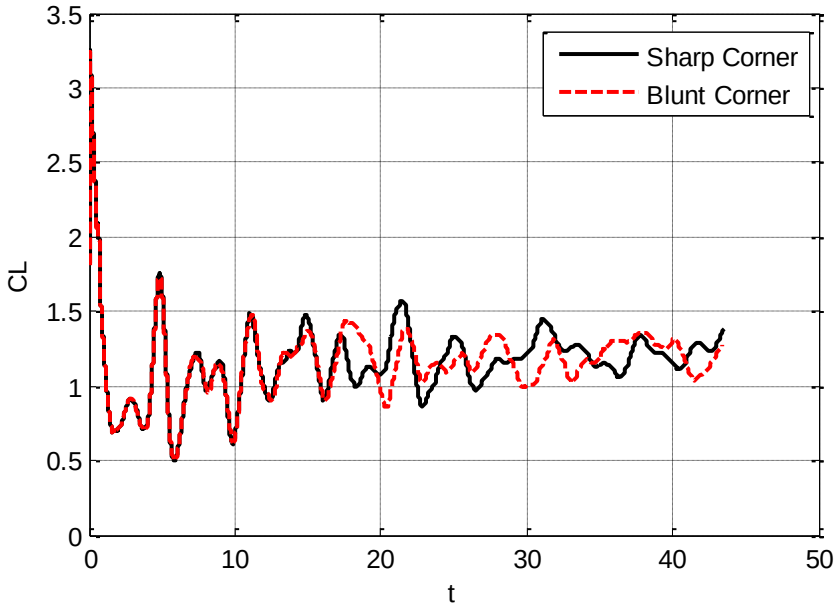

Figure 4-6 C_L comparison between the sharp corner and blunt corner geometry

4.3 2D Simulation Results

With all the numerical uncertainties minimized, the 2D simulation was performed at all AOAs, and the results of lift coefficients are shown in Figure 4-6. It is quite similar to the 2D simulation results of the smooth airfoil. For lower AOAs, the agreement between 2D CFD and experimental results is pretty decent. In the mid-AOA range, there is mild overestimation which keeps getting larger as the AOA increases. For higher AOAs, where the airfoil stalls in the experiment, the lift coefficients computed by 2D simulation tend to keep increasing, when the AOA reaches 16 degrees, there is already a 60% over prediction.

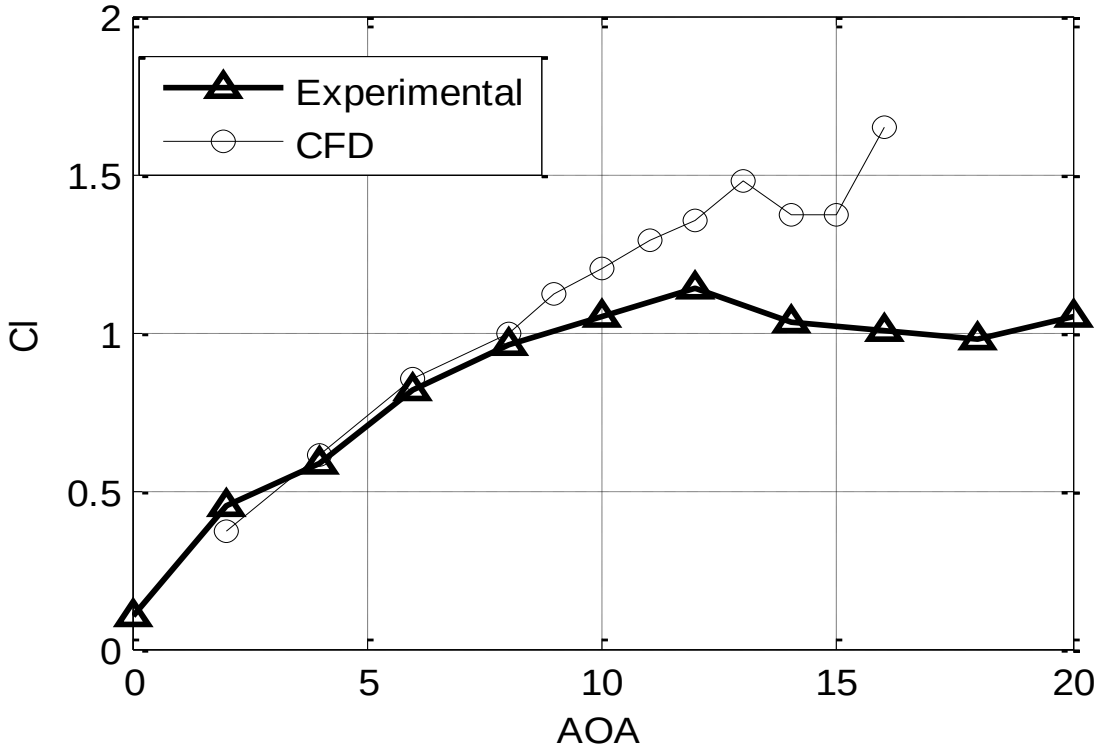

Figure 4-7 2D CFD time-averaged lift coefficients compared with experimental results

A closer look at the instantaneous vorticity distribution at AOA = 16deg (Figure 4-7) also revealed that the vorticity were mainly concentrated in large vortices, and there was almost no vorticity distributed outside those large structures. These large vortices propagated along the upper surface and thus large part of the fluid flow was still non-reversed.

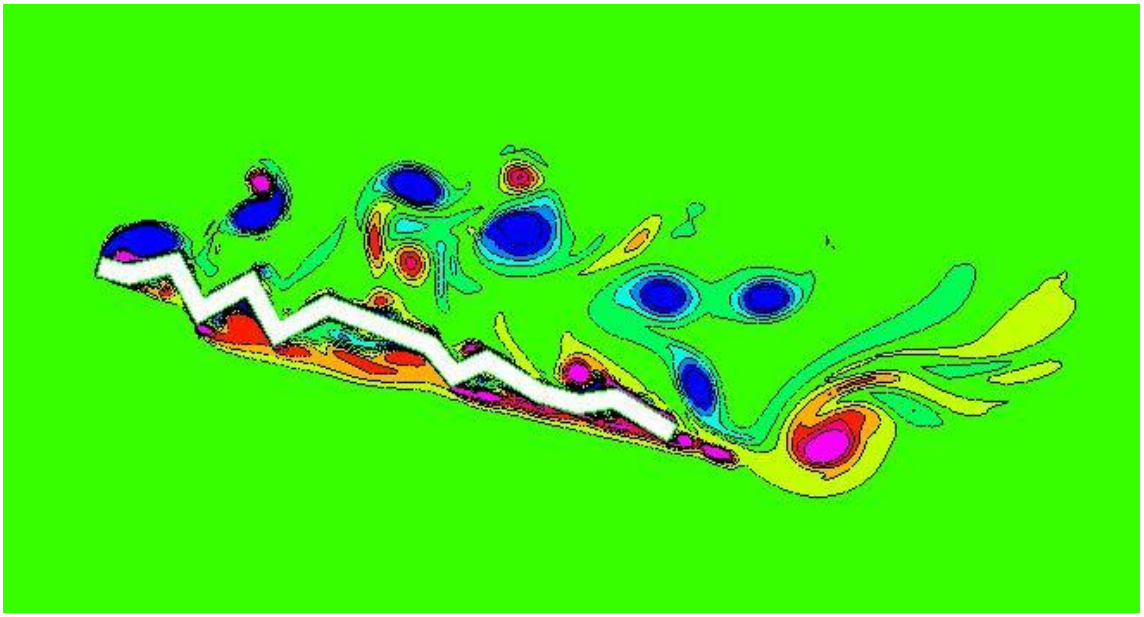

Figure 4-8 Instantaneous vorticity field by 2D simulation

Again, some incorrect voticity behavior seemed to cause the completely wrong results in lift coefficients by 2D simulation, and to further confirm the speculation, a 3D simulation was needed.

4.4 3D Simulation of Corrugated Dragonfly Airfoil @AOA=16 deg

The 3D mesh was created via the extrusion of the coarse mesh, with a chord length as the spanwise direction, and the final mesh size is 2,576,320 cells. The same as the treatment of the smooth airfoil, symmetry boundaries were added to both ends of spanwise direction. Other parameters were kept the same as the 2D simulation.

Figure 4-8 and Figure 4-9 below show the 3D simulation results of 3D simulation of dragonfly airfoil at AOA =16deg solved by MUSIC and 3rd order spectral difference solver. It can be seen that in the beginning, the 3D results behave similarly to 2D, but later when 3D structures were fully developed, 3D simulation yielded a much less oscillatory lift coefficient history, and the lift coefficient slowly approached the experimental averaged value. When finally the semi-periodic state was reached, 3D simulation obtained very good agreement with the experimental average value.

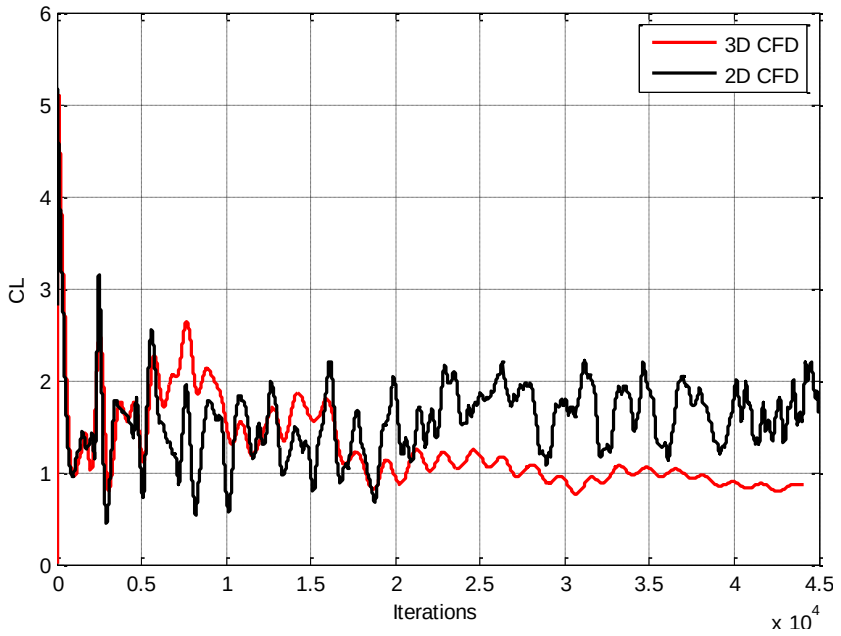

Figure 4-9 Comparison of lift coefficients history @ AOA=16 deg by 2D and 3D simulation by MUSIC

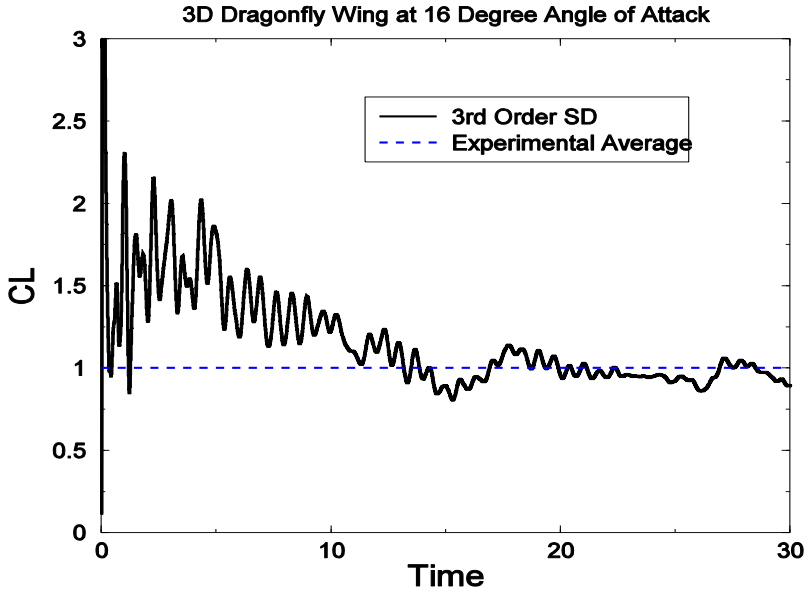

Figure 4-10 lift coefficients history @ AOA=16 deg from 3D simulation by 3rd order spectral difference

The instantaneous vorticity field tells the same story as that in the case of a smooth airfoil, in 3D simulation; the vorticity was spread over the whole area above the airfoil, instead of concentrating in a few large structures, as is shown by Figure 4-10.

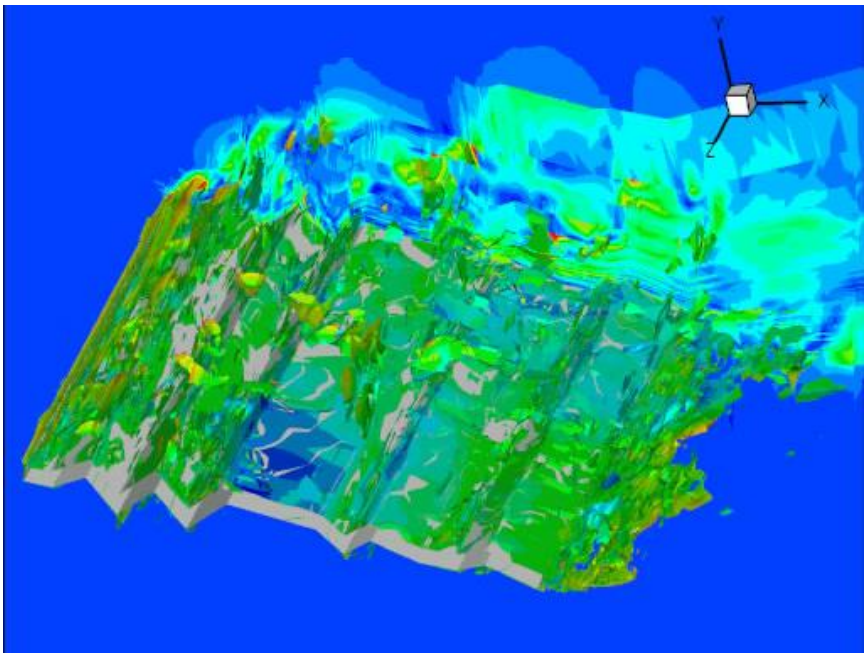

Figure 4-11 Instantaneous vorticity field by 3D simulation of

3rd order spectral difference solver

So, both the simulations on a smooth and a corrugated airfoil ended up with similar conclusion, that 2D simulation is unable to predict the correct stalling behavior at high AOAs, and one possible reason for this is the incorrect vorticity behavior of 2D Navier-Stokes euqaions.

Chapter5

Conclusions

The present numerical study of quasi-two-dimensional flows at low Reynolds number around two different type of airfoil geometries has lead to following conclusions:

1. For low AOAs (less than 7 deg), where the time-averaged flow field is in an attached manner, 2D Navier-Stokes simulation is able to predict the correct lift coefficient along with the pressure distribution very accurately, in spite of the incorrectly predicted small separation bubbles near the trailing edge.
2. For mid-range AOAs (From 7 to 11 deg), where the time-averaged flow field is dominated by the transitional separation bubble, 2D simulation tend to overpredict the length of separation bubble and thus overestimate the lift coefficient, the errors are within 20%.
3. For post-stall AOAs, 2D simulation is unable to predict the stall of the airfoil, both in terms of lift coefficients and flow field structures, while 3D simulation is able to get fairly close to the experimental data in both airfoils simulated.
4. The incapability of 2D simulation for predicting the lift trend at post-stall AOAs can be possibly associated with the incorrect diffusion behavior of the 2D Navier-Stokes equations, in which 3D large scale structures play a vital part.

With the correction of various transition models, several previous study has shown that 2D simulation can perform very well in the mid-range AOAs too, therefore, CFD simulations based on 2D Navier-Stokes equations useful and accurate. However, to predict the stalling and post-stall behaviors correctly, it seems that a 3D simulation is necessary and 2D simulations should not be recommended.

The 3D simulations of the present study used a much less grid resolution than needed by LES/DNS and thus a considerable portion of smaller scale eddies were missing. Therefore, although the current study has uncovered some aspects of the 3D behaviors of the flow, more thorough 3D simulation thorough LES or DNS is needed to further confirm the results when possible.

Bibliography

[1]. Schindel, L. H, "Store Separation," AGARD-AG-202, June 1975
[2]. Grasmeyer, J. M., and Keennon, M. T., "Development of the Black Widow Micro Air Vehicle," AIAA Paper No. 2001-0127, 2001.
[3]. Ifju, P. G., Jenkins, A. D., Ettingers, S., Lian, Y., and Shyy, W., "Flexible-Wing-Based Micro Air Vehicles," AIAA Paper 2002-0705, 2002.
[4]. Jones, K. D., and Platzer, M. F., "Experimental Investigation of the Aerodynamic Characteristics of Flapping-Wing Micro Air Vehicles," AIAA Paper 2003-0418, 2003.
[5]. Shyy, W., Berg, M., and Ljungqvist, D., "Flapping and Flexible Wings for Biological and MicroVehicles," Progress in Aerospace Sciences, Vol. 35, No. 5, 1999, pp. 455–506.
[6]. Marchman III, J. f. and Abtahi, A. A., "Aerodynamics of an Aspect Ratio 8 Wing at Low Reynolds Numbers," Journal of Aircraft, 22(7): 628-634, 1985.
[7]. Lissaman, P. B. S., "Low-Reynolds-Number Airfoils," Annual Review of Fluid Mechnics, Vol. 15, 1983, pp.223-239
[8]. Pines, D. J. and Bohorquez, F., "Challenges Facing Future Micro-Air-Vehicle Development," Journal of Aircraft, Vol. 43, No.2, 2006, pp. 290-304.
[9]. Gopalarathnam, A., Broughton, B. A., McGranahan, B. D., and Selig, M. S., "Design of Low Reynolds Number Airfoils with Trips," Journal of Aircraft, Vol. 40, No.4, 2003, pp. 768-775.
[10]. Okamoto, M. and Azuma, A., "Experimental Study on Aerodynamic Characteristics of Unsteady Wing at Low Reynolds Number," AIAA Journal, Vol. 43, No. 12, 2005, pp. 2526-2536.
[11]. Ekaterinaris, J. A., Chandrasekhara, M. S. and Platzer, M. F., "Analysis of Low Reynolds Number Airfoil Flows," Journal of Aircraft, Vol. 32, No. 3, 1995, pp. 625-630.
[12]. Dini, P. and Maughmer, M. D., "Locally Interactive Laminar Separation Bubble Model," Journal of Aircraft, Vol. 31, No.4, 1994, pp. 802-810.
[13]. Brendel, M. and Mueller T.J., "Boundary Layer Measurements on an Airfoil at Low Reynolds Numbers," Journal of Aircraft, Vol. 22, No.7, 1988, pp. 612-617
[14]. Marchman, J. F., "Aerodynamic Testing at Low Reynolds Numbers," Journal of Aircraft, Vol. 24, No.2, 1987, pp. 107-114
[15]. Hu, H. and Yang, Z., "An Experimental Study of the Laminar Flow Separation on a Low-Reynolds-Number Airfoil," Manuscript submitted to Journal of Fluid Engineering
[16]. Nagamatsu, H.T. and Cuche, D.E., "Low Reynolds Number Aerodynamic Characteristics of Low-Drag NACA 63-208 Airfoil," AIAA 80-1417R, 1980.
[17]. Pohlen, L. J. and Mueller, T. J., "Boundary Layer Characteristics of Miley Airfoil at Low Reynolds Numbers," Journal of Aircraft, Vol. 21, No.9, 1984, pp. 658-664.

[18]. Pelletier, A. and Mueller, T. J., "Effect of Endplates on Two dimensional Airfoil Testing at Low Reynolds Number," Journal of Aircraft, Vol. 38, No. 6, 2001, pp. 1056-1059.
[19]. Broeren, A. P. and Bragg, M. B., "Spanwise Variation in the Unsteady Stalling Flowfields of Two Dimensional Airfoil Models," AIAA Journal, Vol. 39, No. 9, 2001, pp. 1641-1651.
[20]. Liu, H.-T., "Unsteady Aerodynamics of a Wortmann Wing at Low Reynolds Numbers," Journal of Aircraft, Vol. 29, No. 4, 1992, pp. 532-539
[21]. Hansman, R. J. and Craig, A. P., "Low Reynolds Number Tests of NACA 64-210, NACA 0012, and Wortmann FX67-K170 Airfoils in Rain," Journal of Aircraft, Vol. 24, No. 8, 1987, pp. 559-566.
[22]. Zhan, J., Wang, W., Wu, Z. and Wang, J., "Wind-Tunnel Experimental Investigation on a Fix-Wing Micro Air Vehicle," Journal of Aircraft, Vol. 43, No.1, 2006, pp.279-282.
[23]. Scharf, D. F. and Mueller, T. J., "Experimental Study of a Low Reynolds Number Tandem Airfoil Configuration," Journal of Aircraft, Vol. 29, No. 2, 1992, pp. 231-236.
[24]. Granville, P. S., "The Calculation of the Viscous Drag of Bodies of Revolution" David W. Taylor Model Basin, Washington, DC, Rept, 849, 1953.
[25]. Hsiao, F. B. and Hsu, C. C., "Numerical Prediction of Aerodynamic Performance for Low Reynolds Number Airfoils," Journal of Aircraft, Vol. 26, No.7, 1989, pp.689-692.
[26]. Coiro, D. P., "Prediction of Aerodynamic Performance of Airfoils in Low Reynolds Number Flows," Low Reynolds Number Aerodynamics, Springer, Berlin, 1989, pp.13-23.
[27]. Cebeci, T., McIlvaine, M., Chen, H. H. and Liebeck, R. H., "Calculation of Low Reynolds Number Flows at High Angles of Attack," Journal of Aircraft, Vol. 28, No. 4, 1991, pp. 246-252.
[28]. Cebeci, T., Chen, H. H. and Lee, B. P., "Calculation of Three-Dimensional Low Reynolds Number Flows," Journal of Aircraft, Vol. 31, No. 3, 1994, pp. 564-571.
[29]. Shum, Y. K. and Marsden, D. J., "Separation Bubble Model for Low Reynolds Number Airfoil Applications," Journal of Aircraft, Vol. 31, No. 4, 1994, pp. 761-766.
[30]. Lian, Y. and Shyy, W., "Laminar-Turbulent transition of a Low Reynolds Number Rigid or Flexible Airfoil," AIAA Journal, Vol. 45, No.7, 2007, pp.1501-1513.
[31]. Ghia, K. N., Osswald, G. and Ghia, U., "Study of Low-Reynolds Number Separated Flow Past the Wortmann FX 63-137 Airfoil," Low Reynolds Number Aerodynamics, Springer, Berlin, 1989, pp.58-69.
[32]. Liebeck, R. H., ''Design of Subsonic Airfoils for High Lift,'' Journal Aircraft, Vol. 15, No. 9, 1978, pp. 547 - 561.

[33]. Maughmer, M. D., and Somers, D. M., ‘‘Design and Experimental Results for a High-Altitude, Long-Endurance Airfoil,’’ Journal of Aircraft, Vol. 26, No. 2, 1989, pp. 148 - 153.
[34]. Chien, K. Y., “Predictions of Channel and Boundary-Layer Flows with a Low-Reynolds-Number Turbulence Model,” AIAA Paper No. 80-0134R, 1980
[35]. Mueller, T. J., ‘‘Low Reynolds Number Vehicles,’’ AGARDograph 288, Feb. 1985.
[36]. Selig, M. S. and Guglielmo, J. J., “High-Lift Low Reynolds Number Airfoil Design,” Journal of Aircraft, Vol. 34, No. 1, 1997, pp. 72-79.
[37]. Huang, R.F. and Lin, C.L., “Vortex shedding and shear-layer instability of wing at low-Reynolds numbers,” *AIAA Journal,* Vol.**33** (1995), pp. 1398–1430.
[38]. Lin, J. C. Multi and Pauley, L. L., “Low-Reynolds-Number Separation on an Airfoil,” AIAA Journal, Vol.34, No. 8, 1996, pp.1570-1577.
[39]. Patel, V. C., Rodi, W. and Scheuerer, “Turbulence Models for Near-Wall and Low Reynolds Number Flows: A Reiview,” AIAA Journal, Vol. 23, No. 9, 1985, pp. 1308
[40]. Z.J. Wang and R.F. Chen, “Anisotropic Solution Adaptive Viscous Cartesian Grid Method for Turbulence Flow Simulation,” AIAA Journal, Vol. 40, No. 10, Oct. 2002
[41]. Sun, Y., Wang, Z.J. and Liu, Y., “High-Order Multidomain Spectral Difference Method for the Navier-Stokes Equations,” AIAA-2006-0301.
[42]. Delery, J. M., “Physics of Vortical Flows,” Journal of Aircraft Vol. 29, No. 5, 1992, pp. 856-876.
[43]. Rayleigh, W. S., Proc. R. Soc. London Ser. A 93, 148 (1916)
[44]. Taylor, G. I., Philos. Trans. R. Soc. London Ser. A223, 289 (1923)
[45]. Bayly, B. J., “Three-Dimensional centrifugal-type instabilities in inviscid two-dimensional flows,” Phys. Fluids 31 (1), 1988, pp. 56-64
[46]. Bayly, B. J., “Three-Dimensional Instability of Elliptical Flow,” Phys. Rev. Letters, Vol. 57, No. 17 , 1986, pp. 2160-2163.
[47]. M. Tamai, Z. Wang, G. Rajagopalan, H. Hu, and G. He, Aerodynamic Performance of a Corrugated Dragonfly Airfoil Compared with Smooth Airfoils at Low Reynolds Numbers, 45th AIAA Aerospace Sciences Meeting and Exhibit, Reno, Nevada, Jan. 8-11, 2007